Quaternary Science Reviews 215 (2019) 253–271

Contents lists available at ScienceDirect

Quaternary Science Reviews

journal homepage: www.elsevier.com/locate/quascirev

Multiple independent records of local glacier variability on Nuussuaq, West Greenland, during the Holocene

Avriel D. Schweinsberg [a, *], Jason P. Briner [a], Joseph M. Licciardi [b], Ole Bennike [c], Nathaniel A. Lifton [d, e], Brandon L. Graham [a], Nicolás E. Young [f], Joerg M. Schaefer [f], Susan H. Zimmerman [g]

[a] Department of Geology, University at Buffalo, Buffalo, NY 14260, USA
[b] Department of Earth Sciences, University of New Hampshire, Durham, NH 03824, USA
[c] Geological Survey of Denmark and Greenland, Øster Voldgade 10, DK-1350 Copenhagen K, Denmark
[d] Department of Earth, Atmospheric, and Planetary Sciences, Purdue University, West Lafayette, IN 47907, USA
[e] Department of Physics and Astronomy, Purdue University, West Lafayette, IN 47907, USA
[f] Lamont-Doherty Earth Observatory,Columbia University, Palisades, NY, USA
[g] Center for Accelerator Mass Spectrometry, Lawrence Livermore National Laboratory, Livermore, USA

ARTICLE INFO

Article history:
Received 4 November 2018
Received in revised form
8 May 2019
Accepted 10 May 2019

Keywords:
Holocene
Greenland
Mountain glaciers
Lake sediment
Cosmogenic *in situ* ^{14}C
Cosmogenic ^{10}Be
Neoglaciation

ABSTRACT

The sensitivity of mountain glaciers to small-scale climate fluctuations makes records of their past extent among the best proxies for identifying spatio-temporal climate variability. Here we build on the few existing Holocene records of local glacier change in Greenland by using three independent geochronological methods—proglacial lake sediment analysis, cosmogenic ^{10}Be surface-exposure dating, and *in situ* ^{14}C burial modeling—to reconstruct continuous records of Holocene glacier variability on Nuussuaq, West Greenland. ^{10}Be ages of perched boulders indicate eastern Nuussuaq was deglaciated between ~11.0 and 10.5 ka. Radiocarbon-dated sediments from two lakes on Nuussuaq contain mineral-rich layers between ~9.6 and 9.0 and ~8.7–8.0 cal ka BP that may be correlative with nearby ice sheet moraines deposited in the early Holocene. Multiple proxies for glacier size indicate frequent, high-amplitude glacier fluctuations superimposed on net glacier growth during the late Holocene, with significant ice expansion phases at ~3.7 ka, 2.8 ka, and throughout the past ~2 ka. Mean ^{10}Be ages from five nested moraine crests confirm that local glacier extents on Nuussuaq culminated during both the Little Ice Age [~1470 C.E. ($n = 3$) and 1750 C.E. ($n = 3$)] and the preceding centuries (~520–1320 C.E.; $n = 11$). Results reveal that local glaciers on Nuussuaq episodically advanced and retreated at centennial timescales throughout the Holocene, most likely in response to regional climate changes in West Greenland superimposed on the progressive insolation-driven cooling trend in the Northern Hemisphere. Our new ^{10}Be moraine chronologies coupled with other glacier-size proxies corroborate an emerging pattern of significant summer cooling and glacier expansion in the centuries prior to the Little Ice Age in the Arctic.

1. Introduction

As concerns grow regarding the response of the Greenland Ice Sheet (GrIS) to rising global temperatures (Vaughan et al., 2013), it is increasingly important to elucidate the spatio-temporal climate variability of the Arctic and to define limits for the sensitivity of ice masses to climate change. Mountain glaciers and ice caps (GIC) peripheral to the GrIS react sensitively to short-lived climate variations, and reconstructions of their past extents provide information critical for understanding and predicting current and future GIC behavior (Oerlemans, 2005). Furthermore, geological reconstructions of GIC located adjacent to the GrIS may serve as proxies for the mass balance history of the ice sheet itself (e.g., Levy et al., 2014).

Well-dated records of late Holocene alpine glacier fluctuations have been developed from various regions in the Northern Hemisphere (e.g., Davis et al., 2009), such as Alaska (e.g., Barclay et al., 2009; Badding et al., 2013; Solomina et al., 2015, 2016 and

* Corresponding author.
E-mail address: avrielsc@buffalo.edu (A.D. Schweinsberg).

https://doi.org/10.1016/j.quascirev.2019.05.007
0277-3791/

references therein), Canada (e.g., Luckman, 2000; Menounos et al., 2009; Clague et al., 2010), Scandinavia (Nesje, 2009) and the Alps (e.g., Ivy-Ochs et al., 2009; Schimmelpfennig et al., 2012; Le Roy et al., 2017). However, direct evidence for past changes in local glacier extents in Greenland remains sparse (Kelly and Lowell, 2009). In Greenland, the vast majority of GIC and the GrIS margin are fronted by large and extensive moraines that were deposited during a recent period of glacier advance, known as the Little Ice Age (LIA, 1250–1900 C.E.; Grove, 1988). Due to the destructive nature of successive glacial advances (Gibbons et al., 1984), most geomorphic evidence related to earlier phases of ice growth and retreat has been obliterated, and obtaining direct evidence for GIC fluctuations prior to the last few centuries is challenging. Only a few locations in West Greenland preserve local glacier moraines deposited outboard of the LIA maximum extent that are mapped as, or dated to, the middle or late Holocene (Weidick, 1968; Sugden, 1972; Kelly and Lowell, 2009). Continuous records of Holocene GIC fluctuations are equally rare, with a limited number of available lake sediment-based studies in East Greenland (Levy et al., 2014; Balasico et al., 2015; Van der Bilt et al., 2018) and West Greenland (Larsen et al., 2017; Schweinsberg et al., 2017, 2018). This dearth of pre-LIA Holocene glacier reconstructions limits our understanding of GIC behavior during the Holocene, including climatic transitions that were both warmer and cooler than present (Kaufman et al., 2004; Marcott et al., 2013).

Several recent cosmogenic nuclide surface-exposure dating investigations have placed direct age constraints on late Holocene alpine glacier moraines in West Greenland (Young et al., 2015; Jomelli et al., 2016) and in Arctic Canada (Young et al., 2015; Crump et al., 2017). These pre-LIA moraine sequences provide evidence that some older local glacier extents were roughly equal to ice limits attained during the LIA (Weidick, 1968; Kelly and Lowell, 2009; Young et al., 2015; Jomelli et al., 2016). Additionally, these chronologies suggest that climatic conditions favorable for glacier growth occurred centuries to millennia before the LIA interval, and coincident with the Medieval Warm Period in Europe (MWP; 950–1250 C.E.; Lamb, 1965). However, without additional age control from other late Holocene moraines and records of GIC changes earlier in the Holocene, it remains challenging to assess the regional significance of expanded glaciers at this time.

The aim of this study is to reconstruct GIC fluctuations on Nuussuaq, West Greenland, using multiple independent proxies to gain insight on the spatio-temporal variability of GIC change during the Holocene. We expand on recent work by Schweinsberg et al. (2017) who presented a continuous record of Holocene GIC variability derived from lake sediment analyses (Sikuiui Lake, Fig. 1), ^{10}Be ages of perched boulders, and radiocarbon dating of formerly ice-entombed *in situ* moss in this region. We supplement work done by Schweinsberg et al. (2017) by combining: 1) lacustrine archives from proglacial Pauiaivik Lake and Saqqap Tasersua, 2) ^{10}Be ages of additional perched boulders and from local glacier moraines (Saqqap Tasersua moraines), and 3) modeled exposure-burial scenarios derived from pairing new *in situ* ^{14}C measurements in high-altitude bedrock surfaces with previously radiocarbon-dated *in situ* moss (Schweinsberg et al., 2017).

2. Nuussuaq

2.1. Study area and regional setting

The study region encompasses eastern Nuussuaq between 70 and 71°N and 50–52°W in central West Greenland (Fig. 1). Bedrock lithologies at our field sites comprise Precambrian basement rocks (~3.0–2.8 billion years old), including granites and orthogneisses, with suitable quartz abundances for *in situ* cosmogenic ^{10}Be and ^{14}C surface-exposure dating (Weidick and Bennike, 2007; Larsen et al., 2016). Eastern Nuussuaq is characterized by heavily glaciated uplands (summits reaching c. 2000 m a.s.l.) incised by large and overdeepened southeast-northwest trending valleys. Widespread unvegetated moraines and trimlines mark recent glacier retreat.

Weathered bedrock tors and autochthonous blockfields are found on the uplands of Nuussuaq, and suggest minimal glacial sculpting on these surfaces during previous episodes of ice cover by the GrIS and/or GIC. In response to recent warming, the lateral retreat of ice caps across this high-elevation terrain reveals undisturbed patterned ground, and provides additional evidence that the majority of local ice in these highlands is frozen to its bed (i.e., cold-based; Falconer, 1966). In contrast, significant glacial erosion is associated with the ice-cap outlet glaciers that carve deep tributary valleys into the trunk valley walls, and deposit large, sharp-crested moraines on the valley floor (Fig. 1). We capitalize on these varying glacial regimes by combining methods that require either sufficient glacial erosion (lake sediment analysis, ^{10}Be dating) or no erosion (radiocarbon dating of *in situ* moss, *in situ* ^{14}C burial dating), to provide a comprehensive record of Holocene GIC change on Nuussuaq.

Pauiaivik Lake (70° 20′N, 51° 27′W) and Saqqap Tasersua (70° 11′N, 51° 30′W) are located in the interior of Nuussuaq and approximately 16 km apart from each other (Fig. 1). Pauiaivik Lake measures 1.5 × 0.5 km and is fed by meltwater from an outlet glacier of the Qangattaq ice cap (Fig. 2). Distinct moraines defined by sharp crests are located in front of the present-day glacier that provides sediment input to the lake, particularly in the eastern sub-basin where our coring site is located. The coring site is approximately 1 km from the modern glacier margin (2016 C.E.) and 0.5 km from the unvegetated moraines fronting the glacier. The close proximity of the coring site to the glacier results in a minimal sediment transport distance; therefore, Pauiaivik Lake is ideally situated to capture and preserve a detailed sedimentary record of past glacier activity.

Saqqap Tasersua is a northwest-southeast trending 40 km-long proglacial lake that bisects the interior of Nuussuaq (Fig. 1). Along the lake, Saqqap Tasersua is fed by numerous ice-cap outlet glaciers fronted by large unvegetated moraines, many of which are located along the lakeshore. Coring was performed in the easternmost embayment of Saqqap Tasersua; this small circular sub-basin measures 0.02 km^2 and is protected from the remainder of the lake by a shallow 90 m-wide sill. The embayment is part of a chain-lake system, with glacial meltwater being sourced primarily from the outlet glaciers flanking the northern side of the independent ice cap to the southeast. The coring site may also be influenced by glacial activity occurring in the larger part of the lake to the northwest. Since the sub-basin of Saqqap Tasersua that we cored is fed by multiple ice-cap outlet glaciers, we suggest that the glacier history reconstructed from this site represents an integrated signal of glacier change.

2.2. Holocene glacial history

It is postulated that the GrIS overran Nuussuaq during the global Last Glacial Maximum (LGM, 26.5–19 ka; Clark et al., 2009) resulting in the coalescence of local glaciers with the adjacent ice sheet margins (Funder et al., 2011; Roberts et al., 2013; Beel et al., 2016). Following the LGM, the Uummannaq ice stream retreated between ~11 and 10 ka along the northern flank of Nuussuaq (Roberts et al., 2013). The most direct limit on the timing of local deglaciation comes from ^{10}Be ages of perched boulders that date to ~10.7 ka in our study area (Roberts et al., 2013; Schweinsberg et al., 2017; O'Hara et al., 2017). These ages are supported by minimum-limiting radiocarbon ages of ~11.8 and 10.0 cal ka BP from

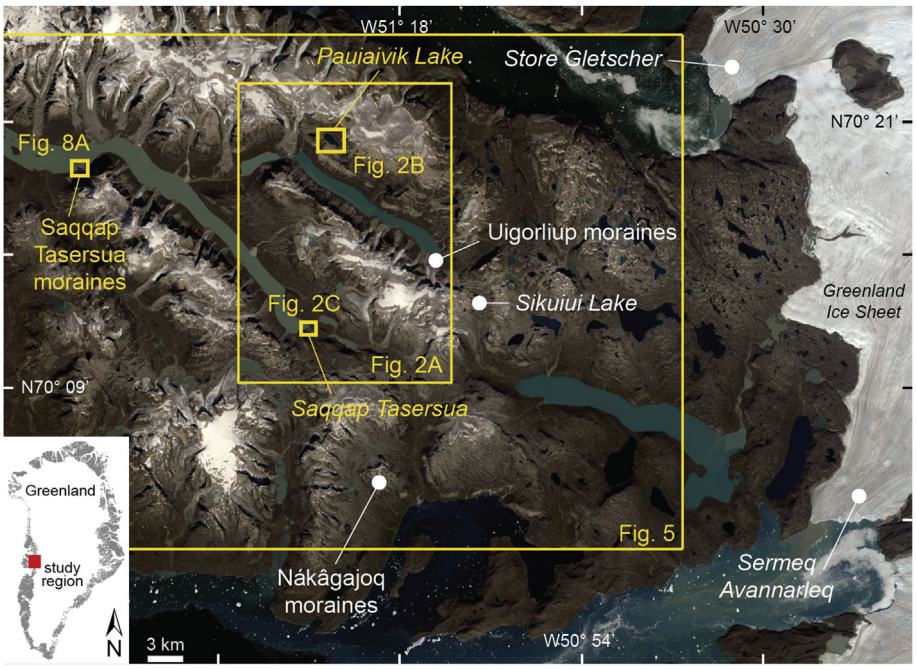

Fig. 1. Map of eastern Nuussuaq showing study sites and localities mentioned in the text. Yellow boxes refer to sites in this study; white circles demarcate previous work (Young et al., 2015; O'Hara et al., 2017; Schweinsberg et al., 2017). Inset map shows Greenland with the study region highlighted in red. Base map is a natural color composite (RGB; 432) from a Landsat8 scene acquired on 31 July, 2016. (For interpretation of the references to color in this figure legend, the reader is referred to the Web version of this article.)

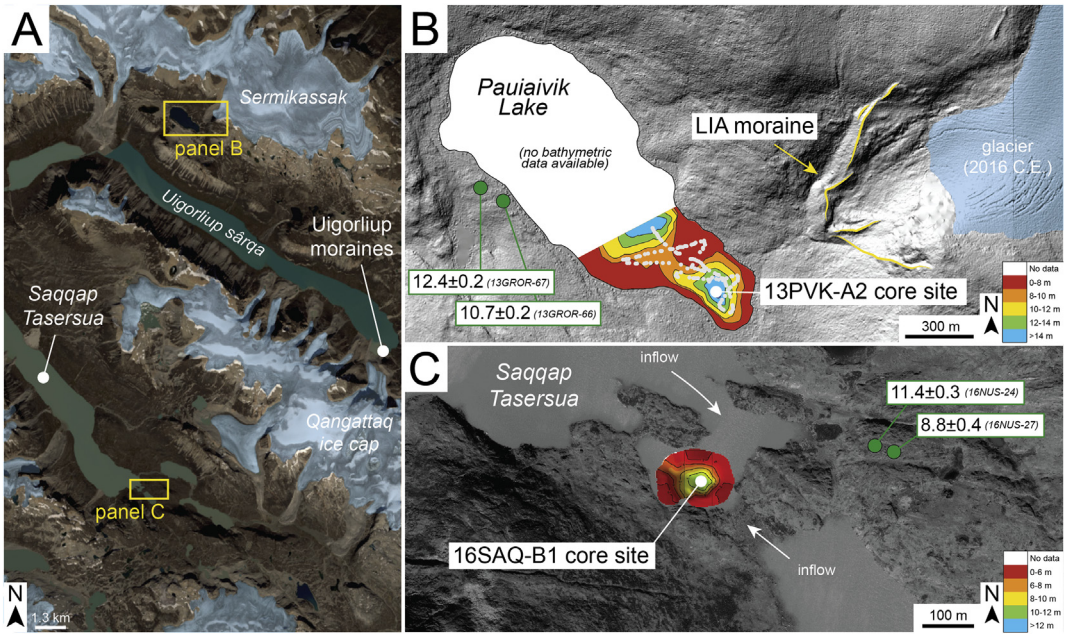

Fig. 2. Proglacial lake study sites and bathymetric maps. **A)** Central part of our field area with study sites indicated by yellow boxes. 2016 C.E. ice extent is shaded blue. **B)** Bathymetric map for Pauiaivik Lake superimposed on the ArcticDEM (Noh and Howat, 2015). Bathymetric data points are marked by small gray circles. ^{10}Be ages of sampled boulders are denoted by green circles (Tables 3 and 4). Yellow lines mark the historical (LIA) moraine; the 2016 C.E. glacier extent is highlighted in blue - this glacier is the primary meltwater source to Pauiaivik Lake. **C)** Bathymetry data for Saqqap Tasersua overlain on a WorldView-2 panchromatic image. Bathymetric contours are two meters. Coring site (16SAQ-B1) is located in the small, easternmost embayment of Saqqap Tasersua. ^{10}Be ages of sampled boulders are illustrated by the green circles (Tables 3 and 4). (For interpretation of the references to color in this figure legend, the reader is referred to the Web version of this article.)

western and eastern Nuussuaq, respectively (Weidick, 1968; Bennike, 2000), and by numerous radiocarbon and ^{10}Be ages that constrain deglaciation of the Disko Bugt region immediately to the south to between ~11 and 10 ka (Kelley et al., 2013, 2015 and references therein).

The overall pattern of retreat in West Greenland during the early Holocene was punctuated by re-advances and stillstands of the GrIS margin in response to early Holocene climate events (e.g., Weidick and Bennike, 2007; Young et al., 2013a; Cronauer et al., 2016). The Fjord Stade moraines dated near our field area imply that the GrIS

margin responded to early Holocene abrupt climate events at ~9.3 and 8.2 ka (Young et al., 2013a); however, it remains unclear whether regional GIC also responded to these abrupt cooling episodes. ^{10}Be ages of the Nákâgajoq moraines near the south coast of Nuussuaq suggest a possible earlier advance/stillstand of local glaciers at 10.6 ± 0.3 ka (Fig. 1; O'Hara et al., 2017). It is also possible that the Nákâgajoq moraines are correlative to the nearby Disko Stade moraines in central West Greenland (Ingólfsson et al., 1990); however, the age of these moraines have yet to be precisely determined, and are presently estimated at ~12 ka (Jomelli et al., 2016). Mountain glacier fluctuations reconstructed from Sikuiui Lake on Nuussuaq may record a GIC advance between ~8.8 and 8.0 ka that is correlative with nearby GrIS moraine chronologies (Fig. 1; Schweinsberg et al., 2017).

Previous work suggests Nuussuaq GIC readvanced at ~5 ka, following the regional Holocene Thermal Maximum (Briner et al., 2016; Schweinsberg et al., 2017). Subsequent GIC advances are documented at ~3.7, 2.9, 1.7 and 1.4 ka, with the most significant intervals of summer cooling and glacier growth taking place between ~4.0 and 3.5 ka, and throughout the last ~2 ka (Young et al., 2015; Schweinsberg et al., 2017). The timing of these late Holocene glacier advances is similar to glacier fluctuations documented elsewhere in Greenland (Balascio et al., 2015; Larsen et al., 2017; Farnsworth et al., 2018; Van der Bilt et al., 2018), Baffin Island (e.g., Thomas et al., 2010; Miller et al., 2013a,b; Margreth et al., 2014; Crump et al., 2017), Iceland (e.g., Larsen et al., 2013), Scandinavia (Nesje, 2009), Svalbard (Miller et al., 2017), and farther afield (e.g., Solomina et al., 2015, 2016).

Most local glacier moraines preserved on Nuussuaq are undated, although fresh and unvegetated moraines are generally considered to represent the LIA maximum in West Greenland (Weidick, 1968; Kelly and Lowell, 2009). Mountain glacier deposits located directly outboard of LIA moraines have been previously described on Nuussuaq (Heim, 1911; Weidick, 1968; Young et al., 2015) and are found near Saqqaq on the south coast of Nuussuaq, in Saputit valley, and near Qaersuarssuk (Weidick, 1968). Prior to this study, the only late Holocene moraines on Nuussuaq with direct age control were the Uigorliup moraines (Fig. 1; Young et al., 2015); a moraine crest beyond unvegetated moraines attributed to the LIA dated to ~1160 C.E using cosmogenic ^{10}Be surface-exposure dating. The age of the Uigorliup moraines is similar to other ^{10}Be and ^{36}Cl-dated alpine glacier moraines in the Baffin Bay region; local glacier moraines in Naqsaq valley, Baffin Island, date between ~1070 and 1700 C.E. ($n = 19$), suggesting that Naqsaq glacier reached a position similar to its LIA extent as early as ~1070 C.E. (Young et al., 2015). Similarly, moraines in Ayr Lake valley, Baffin Island, date to ~1240 C.E. ($n = 3$; Young et al., 2015), and moraines fronting Lyngmarksbræen on Disko island date to ~1200 C.E. ("M2" of Jomelli et al., 2016). To build on these chronologies, a primary objective of this study is to identify and date additional moraine sequences that may correspond to glacier culminations in the late Holocene but earlier than the LIA.

3. Materials and methods

3.1. Sediment coring and analysis

Proglacial Pauiaivik Lake and Saqqap Tasersua were cored in summer 2013 and 2016, respectively, to develop a continuous history of local glaciation during the Holocene (Figs. 1 and 2). Prior to coring, lake bathymetry was surveyed using a Garmin GPSMAP 400 series GPS receiver connected to a dual beam depth transducer (Pauiaivik Lake) and a Humminbird ONIX 10 fishfinder (Saqqap Tasersua). Bathymetric maps were created by importing GPS-derived waypoints into ArcGIS 10.1 (Pauiaivik Lake) and in the field using Autochart Live (Saqqap Tasersua) where contours were automatically generated (Fig. 2). Sediment core 13PVK-A2 was recovered from Pauiaivik Lake using a modified Universal Coring system (Nesje, 1992). Coring was executed in Saqqap Tasersua (16SAQ-B1) using a Nesje-style percussion-piston coring device, and was hammered until refusal to ensure maximum sediment recovery. In sediment core 13PVK-A2, the sediment-water interface was preserved, and water above the surface sediments was drained and subsequently packed with foam and capped before transport (see Table 1).

Sediment cores were shipped to the National Lacustrine Core Facility (LacCore) at the University of Minnesota, Minneapolis, MN, for core splitting and nondestructive core analyses. Sediment core density was measured at 0.2 cm intervals on a Geotek MSCL-S automated core logger, and magnetic susceptibility (MS), a measure of the relative amount of minerogenic material in the sediment, was performed on core halves at 0.2 cm contiguous intervals using a Geotek MSCL-XYZ automated core logger. Following analyses at LacCore, split cores were analyzed using an Itrax X-ray fluorescence (XRF) core scanner located at the University of Massachusetts-Amherst, Amherst, MA, to determine elemental concentrations. XRF scans were carried out using a molybdenum (Mo) tube with a downcore resolution of 1.0 mm for each sediment core.

We used two measurements as proxies for organic matter content in the lake sediments. Pauiaivik Lake sediments were subsampled at contiguous 0.5 cm intervals for weight loss-on-ignition (LOI, burn at 550 °C) at the University at Buffalo. For Saqqap Tasersua lake sediments, visible reflectance spectroscopy (VIS-RS) was used to measure concentrations of chlorophyll α and its degradation products (collectively classified as chlorins). VIS-RS measurements were performed at 0.5 cm intervals on the split core face of 16SAQ-B1 using a Konica Minola CM-2600d spectrometer attached to the Geotek MSCL-XYZ instrument at LacCore. Calibrated reference spectra were measured at 10 nm intervals between 360 and 740 nm, and total chlorin was determined by the Relative Absorption Band Depth between 660 and 670 nm ($RABD_{660;670}$) following methods outlined in previous studies (e.g., Rein and Sirocko, 2002; Wolfe et al., 2006; Axford et al., 2009; Boldt et al., 2015).

Macrofossils for radiocarbon dating were picked, cleaned with de-ionized water, and sent to the National Ocean Sciences Accelerator Mass Spectrometry Facility (NOSAMS) at the Woods Hole Oceanographic Institution for accelerator mass spectrometry (AMS) radiocarbon age determinations. The humic acid fraction was extracted from bulk sediments for AMS analysis in Pauiaivik Lake sediments where macrofossils were absent ($n = 4$; Table 2). All AMS radiocarbon results were calibrated using CALIB v. 7.0 with the INTCAL13 calibration curve (Stuiver et al., 2005; Reimer et al., 2013), and radiocarbon ages are reported as the median of the 2σ range ± half of the 2σ range (Table 2). Paired analyses of bulk sediment and macrofossils from 29.0 to 1.75 cm depth were obtained in 13PVK-A2 to identify the age offset between bulk sediment and macrofossil radiocarbon ages, and to subsequently correct unpaired bulk sediment radiocarbon ages (Kaplan et al., 2002).

Age-depth models for 13PVK-A2 and 16SAQ-B1 sediment cores were generated using a smooth spline interpolation between radiocarbon ages with the basal age tied to a mean ^{10}Be age for regional deglaciation of 10.8 ± 0.4 ka [$n = 8$; this study (see below) and Schweinsberg et al., 2017]. Age-depth relationships are generated using the CLAM code version 2.2 modeling package (Blaauw, 2010) developed for the open-source statistical program R (v. 3.0.1; R Development Core Team, 2012). We use a smooth spline interpolation (default smoothing value of 0.2) for the entirety of the

Table 1
Lake sediment core metadata.

Lake name	Core ID	Latitude (°N)	Longitude (°W)	Elevation (m a.s.l.)	Water depth (m)	Core length (cm)	Number of ^{14}C ages
Saqqap Tasersua	16SAQ-B1	70.19594	51.50031	245	10.80	252.0	9
Pauiaivik Lake	13PVK-A2	70.33596	51.44075	859	14.55	56.5	10

Table 2
Radiocarbon ages from lake sediment cores.

Core ID	Depth (cm)	Lab Number	Material dated	Fraction modern	δ13C (‰PDB)	Radiocarbon age (14C yr BP)	Calibrated age (cal yr BP with 2σ age range)[a]
Saqqap Tasersua							
16SAQ-B1	27.5	OS-132525	aquatic macrofossils	0.7507	−27.10	2300 ± 15	2340 (2318–2349)
16SAQ-B1	38.0	OS-132526	aquatic macrofossils	0.6551	−26.47	3400 ± 15	3650 (3606–3693)
16SAQ-B1	48.8	OS-131000	aquatic macrofossils	0.6244	−30.93	3780 ± 20	4150 (4089–4183)
16SAQ-B1	66.8	OS-131001	aquatic macrofossils	0.5617	−28.94	4630 ± 20	5420 (5383–5448)
16SAQ-B1	68.5	OS-131002	aquatic macrofossils	0.5750	−27.48	4450 ± 20	5060 (4971–5070)
16SAQ-B1	81.5	OS-132527	aquatic macrofossils	0.5133	−28.51	5360 ± 20	6180 (6172–6216)
16SAQ-B1	106.5	OS-132528	aquatic macrofossils	0.4286	−25.77	6810 ± 25	7650 (7605–7683)
16SAQ-B1	150.8	OS-131003	aquatic macrofossils	0.3682	−26.83	8030 ± 40	8900 (8760–9024)
16SAQ-B1	182.0	OS-132529	aquatic macrofossils	0.3237	−24.59	9060 ± 30	10230 (10194–10247)
Pauiaivik Lake							
13PVK-A2	1.75	OS-110848	aquatic macrofossils	0.9333	−29.43	555 ± 40	580 (515–647)
13PVK-A2	1.75	OS-112362	bulk sediment	0.7766	−29.42	2030 ± 25	1980 (1920–2058)
13PVK-A2	9.50	OS-112363	bulk sediment	0.7387	−27.31	2430 ± 20	2450 (2358–2495)
13PVK-A2	10.75	OS-110849	aquatic macrofossils	0.4291	−36.40	6800 ± 35	7640 (7586–7683)
13PVK-A2	11.25	OS-112361	aquatic macrofossils	0.7533	−23.62	2280 ± 25	2320 (2304–2349)
13PVK-A2	21.00	OS-116946	bulk sediment	0.5812	−23.94	4360 ± 20	4920 (4860–4971)
13PVK-A2	29.00	OS-111003	aquatic macrofossils	0.5149	−24.29	5330 ± 80	6110 (5981–6280)
13PVK-A2	29.00	OS-112364	bulk sediment	0.4916	−22.05	5700 ± 25	6480 (6411–6549)
13PVK-A2	33.75	OS-110850	aquatic macrofossils	0.4528	−23.22	6360 ± 35	7290 (7244–7340)
13PVK-A2	42.25	OS-110851	aquatic macrofossils	0.3689	−24.02	8010 ± 50	8880 (8700–9016)

[a] Calibrated radiocarbon ages are expressed as the median probability and 2σ age range. In the instance of two or more possible age ranges, the range with the highest probability is reported.

13PVK-A2 age model and for the upper 182 cm of 16SAQ-B1. A linear regression is used for the section of 16SAQ-B1 below 182 cm depth (lowermost radiocarbon age; Table 2).

Principal component analysis (PCA) was carried out on 10 measured variables using Matlab R2017b for Windows. The 10 parameters included seven geochemical element counts (Si, K/Ti, Ca, Mn, Fe, Rb and Sr) from the XRF scans as well as MS, density, and LOI (Pauiaivik Lake) or chlorin (Saqqap Tasersua). These elements were selected based on their high signal-to-noise ratio, their presence in siliciclastic sediments, and previous studies that have identified them as useful for reconstructing minerogenic input from bedrock erosion (Bakke et al., 2013; Balascio et al., 2015; Røthe et al., 2015; De Wet et al., 2017). The K/Ti ratio was used rather than Ti and K separately to remove fluctuations related to changing water content following previous studies (e.g., Vasskog et al., 2012). All parameters were downsampled to 0.5 cm intervals using AnalySeries 2.0.6 (Paillard et al., 1996) to achieve comparable resolution to the LOI data prior to PCA.

4. Cosmogenic isotope analysis

4.1. ^{10}Be dating

Samples were collected for cosmogenic ^{10}Be surface-exposure dating (hereafter '^{10}Be dating') to determine the age of the Saqqap Tasersua moraines (hereafter 'ST moraines'; Fig. 1) and to further refine the timing of regional deglaciation of eastern Nuussuaq ("perched boulders"). The ST moraines are a nested set of left-lateral moraines deposited by an unnamed ice-cap outlet glacier that terminates on the shores of lower Saqqap Tasersua (Figs. 1 and 3). We focused our moraine dating efforts on these moraines as they include multiple ridges that exhibit geomorphic characteristics similar to those of the Uigorliup moraines on Nuussuaq (~30 km to the southeast; Fig. 1) and the Naqsaq moraines Baffin Island (Young et al., 2015). Initially identified by Weidick (1968), the inner ST moraines are dominated by fresh, unvegetated sharp-crested ridges that are hypothesized to represent retreat following the most recent LIA culmination. The ST moraines exhibit heavy lichen cover and a subdued ridge morphology (Fig. 3). Nine separate moraine crests comprise the ST moraines targeted for sampling; Moraine 1 (M1) refers to the proximal moraine ridge located directly outboard of the innermost (unsampled) moraine position and Moraine 9 (M9) represents the most distal crest. Only a small segment of M9 is preserved.

Moraines were mapped in the field with a handheld GPS that continuously recorded our position. Samples were collected from boulder surfaces on five of the nine mapped moraine positions (M1, M3, M4, M8 and M9). No boulders suitable for ^{10}Be dating were found on the other moraine crests and/or the moraine segments were too short to generate meaningful sample populations.

Samples for ^{10}Be analysis were collected from the top few centimeters of perched boulders and stable moraine boulders (Fig. 4) using a cordless angle grinder equipped with a 5-inch diamond cutting disc, a sledge hammer and a chisel. Perched boulders are located in high, windswept topographic positions adjacent to the study lakes, and sampled from these positions in order to reduce uncertainty associated with shielding caused by snow or soil cover. Erosion and spalling of the sampled moraine and perched boulder surfaces are considered absent or minimal, as indicated by negligible surface pitting and the preservation of glacial smoothing on most boulder surfaces. Geographic coordinates and sample elevations were obtained using a handheld GPS with approximately ± 5–10 m vertical accuracy. A clinometer was used to measure shielding by surrounding mountains to derive topographic

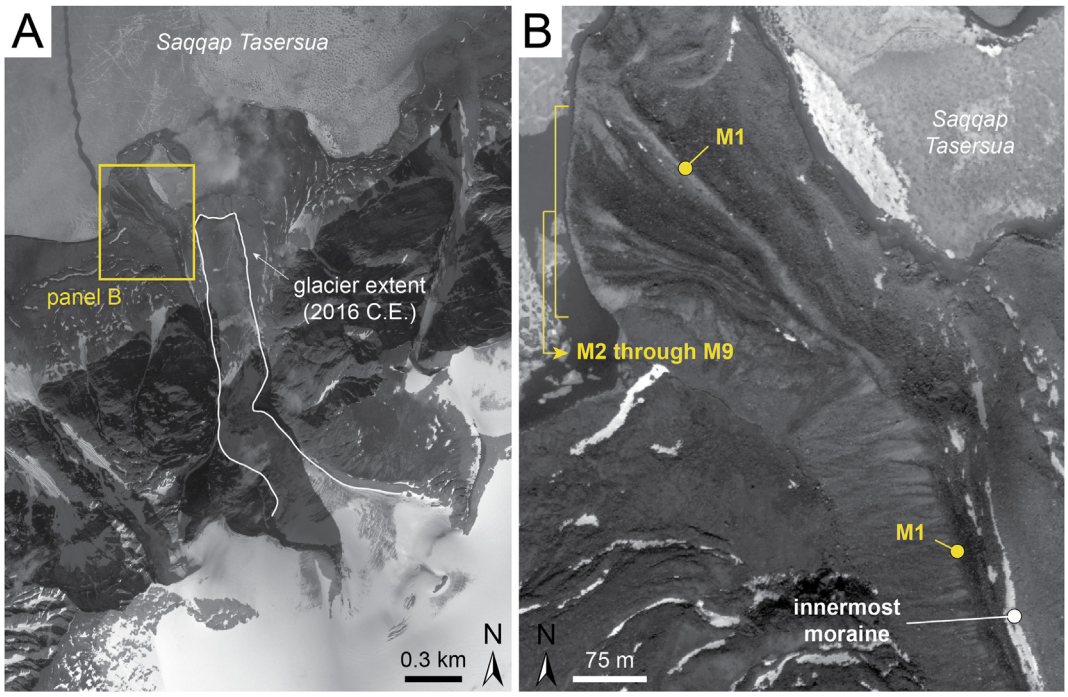

Fig. 3. Saqqap Tasersua moraines and geologic setting. A) Ice-cap outlet glacier that deposited the ST moraines. The 2016 C.E. glacier configuration is shown by the white line. Segments of the right lateral moraines are preserved but were not sampled. B) Close up of the left-lateral ST moraines. The innermost moraine crest is marked with the white dot. The general location of the sampled ST moraine crests is shown; M1 is the most proximal ridge, M9 is the most distal crest.

corrections for each sample. Sample elevations range from ~258 to 289 m a.s.l. (moraine boulders) and from 271 to 933 m a.s.l. (perched boulders); all sample locations are above the local marine limit estimated to be between 40 and 80 m a.s.l. (Weidick, 1968; Weidick and Bennike, 2007). Sample data are provided in Table 3.

All physical processing of the samples was conducted at the University at Buffalo Cosmogenic Isotope Laboratory. Beryllium-isolation chemistry and target packing for the ST moraine boulder samples was completed at the University of New Hampshire Cosmogenic Isotope Laboratory following well-established procedures (e.g., Licciardi, 2000; Corbett et al., 2016). The perched boulder samples were chemically processed at the University at Buffalo. All AMS measurements of $^{10}Be/^{9}Be$ were carried out at the Lawrence Livermore National Laboratory Center for AMS (LLNL-CAMS) with the exception of two perched boulder samples (16NUS-24 and 16NUS-27), which were analyzed at the Purdue Rare Isotope Measurement Laboratory (PRIME Lab), Purdue University, West Lafayette, IN. Each sample ratio was corrected using batch-specific process blank values and reported with 1σ AMS analytical uncertainties. All ^{10}Be ages in this study (and previously published data referred to in the text) are calculated using version 3 of the CRONUS-Earth online exposure age calculator (http://hess.ess.washington.edu/; Balco, 2017) using the regionally calibrated Baffin Bay/Arctic ^{10}Be production rate (Young et al., 2013b) and LSD*n* scaling model (Lifton et al., 2014, Lifton, 2016, Tables 3 and 4). ^{10}Be ages calculated using alternative production rates and scaling schemes are reported in Table 4.

4.1.1. *In situ* ^{14}C

Samples for *in situ* ^{14}C analysis were collected from six recently exposed bedrock surfaces using the same techniques as the ^{10}Be samples. Each bedrock sample was collected adjacent to a previously published radiocarbon-dated *in situ* moss sample (Fig. 5; Schweinsberg et al., 2017). The physical and chemical processing of the *in situ* ^{14}C samples was conducted at PRIME Lab following laboratory procedures detailed in Lifton et al. (2015), and *in situ* ^{14}C concentrations were measured on purified quartz separates (Table 5). Apparent *in situ* ^{14}C exposure ages are calculated after methods described in Hippe and Lifton (2014), and exposure-burial scenarios are modeled in Matlab R2017b following methods and assumptions outlined in Schweinsberg et al. (2018). Each model is sample-specific, and integrates the site-specific time-dependent *in situ* ^{14}C production rate (Borchers et al., 2016; Phillips et al., 2016; Balco, 2017), LSD*n* scaling (Lifton et al., 2014), and the local timing of deglaciation (10.8 ± 0.4 ka; this study; Schweinsberg et al., 2017). Models include scenarios with different ice thicknesses (ranging from 20 to 100 m) to account for the effects of muogenic production beneath thin ice cover (e.g., Hippe, 2017).

5. Results and interpretations

5.1. Proglacial lake sediment records

The chronology of sediment core 13PVK-A2 is based on six and four radiocarbon ages of macrofossils and bulk sediment, respectively (Table 2; Fig. 6A). We interpret the macrofossil radiocarbon age at 10.75 cm depth as an outlier (~7.6 ± 0.1 cal ka BP), and exclude it from the age-depth model. The age offset between the bulk sediment and macrofossil radiocarbon ages at 1.75 cm depth is large (1475 yr BP; Table 2), and not comparable to other studies from western Greenland that show the age offset is typically on the order of 200–400 years (Kaplan et al., 2002; Bennike et al., 2010). In contrast, the paired bulk sediment and macrofossil radiocarbon ages at 29.0 cm depth are comparable (Table 2). Thus, we correct the unpaired bulk sediment radiocarbon ages at 9.5 and 21.0 cm depth in 13PVK-A2 by subtracting the 370-yr offset measured at 29.0 cm depth and consider the bulk sediment age at 1.75 cm depth an outlier. The chronology for sediment core 16SAQ-B1 is established from nine radiocarbon ages of aquatic macrofossils (Fig. 6B). There is a small age reversal between 66.8 and 68.8 cm depth;

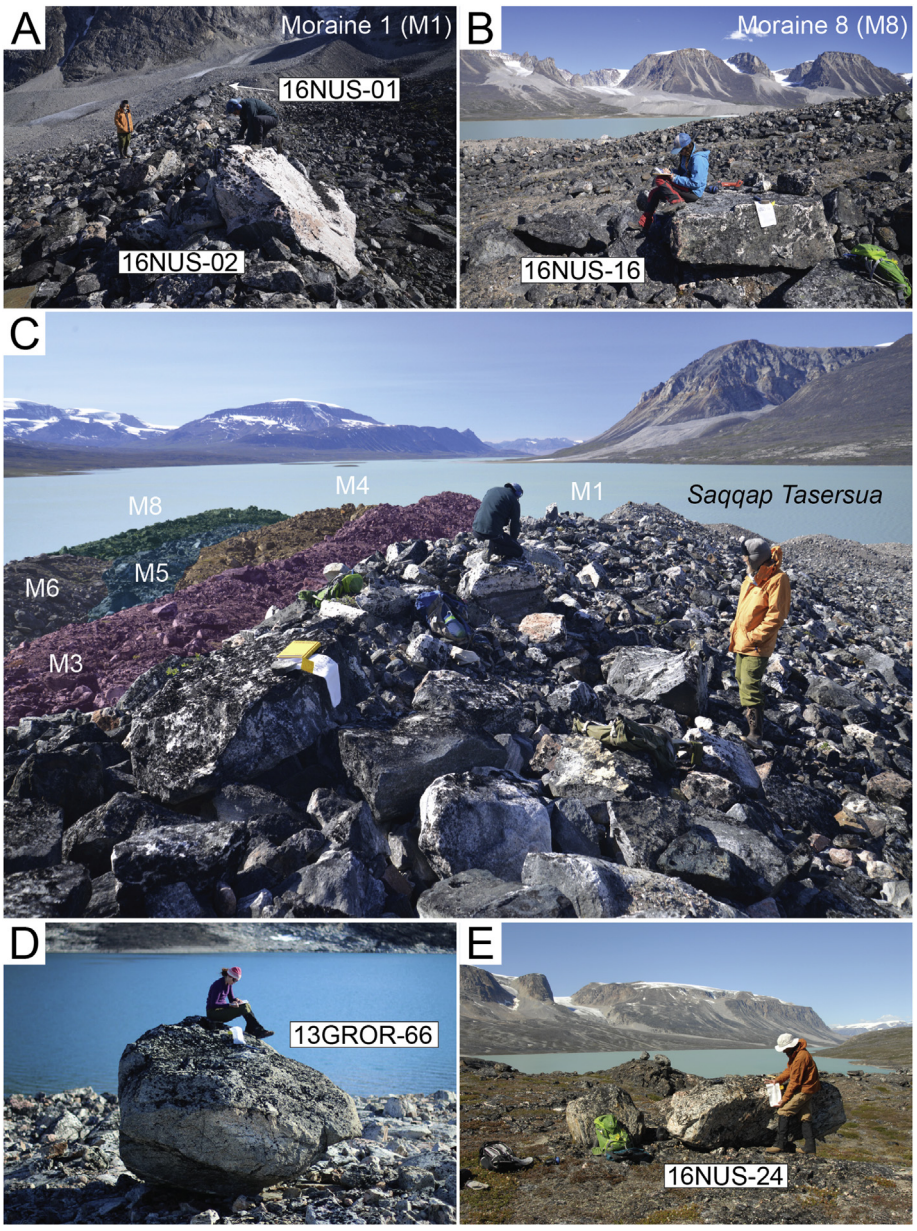

Fig. 4. Representative boulders sampled in this study. **A and B)** Boulders sampled on the Saqqap Tasersua (ST) moraines. **C)** Geomorphic characteristics of the ST moraines. View is from Moraine 1 looking west towards Saqqap Tasersua and western Nuussuaq. Moraines are color-coded to illustrate the crosscutting relationships and differences between moraine positions and morphology. Moraines 2, 7 and 9 are not visible in this photograph. **D and E)** Representative perched boulders sampled for ^{10}Be dating near Pauiaivik Lake (D) and above Saqqap Tasersua (E). (For interpretation of the references to color in this figure legend, the reader is referred to the Web version of this article.)

however, we incorporate both radiocarbon ages in the smooth spline interpolation as a conservative estimate for the true age.

The Pauiaivik Lake and Saqqap Tasersua sediment cores are separated into different lithostratigraphic units based on x-radiograph data and corresponding visual transitions between gray, silt-rich sediment and brown, organic-rich sediment (Fig. 6). The stratigraphy preserved in 16SAQ-B1 is considerably more variable, and the core is subdivided into seven major units (A through G) relative to four sedimentological units in 13PVK-A2. Proxy data, including Itrax elemental data, LOI, MS and density values, were used to guide the unit assignments; sedimentological descriptions and raw downcore data for each sediment core is found in the Supplemental File (Figs. S1 and S2).

PCA is used to detect patterns of variability shared between the measured downcore variables (e.g., Bakke et al., 2013; Balascio et al., 2015; Røthe et al., 2015; De Wet et al., 2017) and serves as our primary tool for documenting mineral-versus organic-rich sediments in our records, and hence interpreting past fluctuations in GIC extent through time. The PCA biplots reveal that most of the geochemical elements exhibit a strong positive correlation with each other and the physical sediment variables, but are negatively correlated with LOI or chlorin (Fig. S3). The first Principal Component (PC1) explains 81% and 56% of the total variance in Pauiaivik Lake and Saqqap Tasersua, respectively, implying that the dataset contains a strong common signal that is reflected by many of the variables (Fig. S3). Most of the geochemical data and physical variables are positively correlated with PC1, whereas LOI or chlorin are negatively correlated. Accordingly, the downcore PC1 scores for both lake sediment records are broadly similar to elemental counts from the Itrax scans and with records of density and MS (Fig. 7,

Table 3
^{10}Be sample information for samples in the Nuussuaq region.

Sample ID	Boulder position	AMS ID	Lat. (°N)	Long. (°W)	Elevation (m a.s.l.)	Thickness (cm)	Shielding correction	Quartz (g)	^{9}Be carrier wt. (g)	^{10}Be/^{9}Be ratio	[Be-10] (atoms g^{-1})	Percent blank corr.
Nuussuaq late Holocene moraines[a]												
16NUS-01	Moraine 1	BE42810	70.315	52.015	267	2.5	0.9704	79.9119	0.1835	9.178E-15 ± 5.473E-16	1417 ± 84	5.2%
16NUS-02	Moraine 1	BE42811	70.315	52.016	258	3.0	0.9704	42.8435	0.1828	5.235E-15 ± 5.007E-16	1501 ± 144	8.8%
16NUS-03	Moraine 1	BE42812	70.315	52.016	268	1.0	0.9704	33.7948	0.1829	4.419E-14 ± 1.083E-15	16077 ± 394	1.1%
16NUS-04	Moraine 1	BE42813	70.315	52.013	289	1.0	0.9639	80.6406	0.1820	9.249E-15 ± 7.327E-16	1403 ± 111	5.2%
16NUS-05	Moraine 1	BE42814	70.315	52.013	288	1.0	0.9639	80.0329	0.1839	8.327E-14 ± 1.874E-15	12862 ± 289	0.6%
16NUS-06	Moraine 3	BE42815	70.315	52.014	284	2.0	0.9693	46.1030	0.1825	6.561E-15 ± 4.322E-16	1746 ± 115	7.2%
16NUS-07	Moraine 3	BE42816	70.315	52.015	277	1.0	0.9699	40.5293	0.1824	1.206E-14 ± 5.870E-16	3647 ± 178	4.0%
16NUS-08	Moraine 3	BE42822	70.315	52.015	279	3.0	0.9711	63.8324	0.1813	1.535E-14 ± 1.018E-15	2927 ± 194	3.2%
16NUS-09	Moraine 3	BE42823	70.315	52.016	272	2.5	0.9711	80.2413	0.1825	1.765E-14 ± 7.224E-16	2698 ± 110	2.8%
16NUS-10	Moraine 4	BE42817	70.315	52.019	268	1.0	0.9673	32.9568	0.1830	1.662E-14 ± 1.105E-15	6205 ± 412	3.0%
16NUS-11	Moraine 4	BE42818	70.315	52.018	268	1.0	0.9649	26.2310	0.1828	1.164E-14 ± 5.959E-16	5455 ± 279	4.2%
16NUS-12	Moraine 4	BE42819	70.315	52.017	273	2.0	0.9673	41.5723	0.1833	1.049E-14 ± 6.078E-16	3110 ± 180	4.6%
16NUS-13	Moraine 4	BE42824	70.315	52.017	273	1.0	0.9641	48.8075	0.1821	2.370E-14 ± 7.932E-16	5943 ± 199	2.1%
16NUS-14	Moraine 8	BE42825	70.314	52.014	264	1.5	0.9645	80.1465	0.1835	1.525E-13 ± 3.382E-15	23426 ± 520	0.3%
16NUS-15	Moraine 8	BE42826	70.314	52.015	266	1.0	0.9645	34.1260	0.1828	2.469E-12 ± 2.454E-14	889168 ± 8837	0.0%
16NUS-16	Moraine 8	BE42827	70.315	52.016	271	1.0	0.9645	73.4526	0.1842	2.925E-14 ± 9.083E-16	4928 ± 153	1.7%
16NUS-17	Moraine 8	BE42828	70.315	52.017	264	1.5	0.9590	23.9755	0.1824	1.298E-14 ± 6.050E-16	6638 ± 309	3.8%
16NUS-18	Moraine 8	BE42829	70.315	52.018	264	1.0	0.9617	24.6222	0.1826	1.160E-14 ± 5.699E-16	5784 ± 284	4.2%
16NUS-19	Moraine 8	BE42830	70.315	52.018	261	2.0	0.9583	80.1212	0.1829	2.916E-14 ± 1.029E-15	4474 ± 158	1.71%
16NUS-20	Moraine 8	BE42831	70.315	52.018	260	2.0	0.9583	37.0337	0.1822	1.405E-14 ± 7.548E-16	4646 ± 250	3.48%
16NUS-21	Moraine 9	BE42832	70.314	52.014	271	2.0	0.9617	59.3638	0.1842	3.483E-14 ± 1.019E-15	7264 ± 213	1.43%
16NUS-22	Moraine 9	BE42833	70.314	52.014	268	2.0	0.9617	21.8218	0.1812	8.948E-15 ± 5.683E-16	4995 ± 317	5.35%
16NUS-23	Moraine 9	BE42834	70.314	52.015	264	1.0	0.9624	16.7310	0.1818	6.445E-15 ± 4.684E-16	4703 ± 342	7.28%
Perched boulder samples near Saqqap Tasersua[b]												
16NUS-24	S. Taser.	148982	70.197	51.490	285	2.0	0.9939	35.7038	0.6046	1.51E-13 ± 3.91E-15	63491 ± 1648	4.75%
16NUS-27	S. Taser.	148983	70.197	51.491	271	2.0	0.9978	40.4312	0.6039	1.31E-13 ± 5.15E-15	48889 ± 1916	4.17%
Perched boulder samples near Pauiaivik Lake[b]												
13GROR-66	P. Lake	BE38146	70.338	51.463	872	1.5	0.9976	20.4773	0.6120	1.363E-13 ± 2.872E-15	111359 ± 2136	1.80%
13GROR-67	P. Lake	BE38147	70.338	51.465	876	2.0	0.9976	20.0138	0.6118	1.653E-13 ± 2.291E-15	103682 ± 1743	1.98%
13GROR-68	P. Lake	BE38148	70.341	51.495	933	2.0	0.9978	19.9978	0.6172	2.990E-13 ± 3.219E-15	126994 ± 2473	1.64%

[a] All ST moraine samples (16NUS-01 through 16NUS-23) were spiked with ~182–184 μg of ^{9}Be prepared from shielded beryl at Lamont-Doherty Earth Observatory ("LDEO carrier 6.0," estimated ^{9}Be concentration: 1006 ppm) in the cosmogenic isotope laboratory at the Univ. of New Hampshire. Four process blanks yielded ^{10}Be/^{9}Be ratios (normalized to standard 07KNSTD3110; Nishiizumi et al., 2007) of 3.1×10^{-16}, 4.4×10^{-16}, 5.9×10^{-16}, and 6.8×10^{-16} (BLK-78, -79, −80, −81, respectively); these ratios equate to ~7694, 5432, 7146 and 8400 ^{10}Be atoms, respectively. AMS 1σ uncertainties ranged from 1.0 to 9.6%.

[b] Perched boulder samples 13GROR-66, -67, and −68 and two samples adjacent to Saqqap Tasersua (16NUS-24 and 16NUS-27) were spiked with ~225–230 μg of ^{9}Be prepared by the GFZ German Research Center for Geosciences ("Phenakite" standard, ^{9}Be concentration: 372 ± 3.5 ppm) at the Univ. at Buffalo. Batch-specific process blanks yielded values of 2.7×10^{-15} (59-Blank) and 6.6×10^{-15} (95-Blank) for Pauiaivik Lake (59-13GROR-66, -67, and −68) and Saqqap Tasersua perched boulder samples (95-16NUS-24, -27), respectively. AMS uncertainties ranged from 1.7 to 3.9% for all deglaciation samples.

Table 4
^{10}Be ages calculated with alternative production rates and scaling models.

Sample ID	^{10}Be ages (years): Arctic/Baffin Bay PR[a]		^{10}Be ages (years): Default CRONUS PR[b]		
	Constant (St)	LSD*n*	Constant (St)	Time-varying (Lm)	LSD*n*
Nuussuaq late Holocene moraines					
16NUS-01 (M1)	260 ± 20	270 ± 20	260 ± 20	250 ± 20	250 ± 20
16NUS-02 (M1)	280 ± 30	290 ± 30	280 ± 30	270 ± 30	260 ± 30
16NUS-03 (M1)	2940 ± 70	2940 ± 20	2910 ± 70	2820 ± 70	2690 ± 70
16NUS-04 (M1)	250 ± 20	260 ± 20	250 ± 20	240 ± 20	240 ± 20
16NUS-05 (M1)	2330 ± 50	2310 ± 50	2300 ± 50	2230 ± 50	2100 ± 50
16NUS-06 (M3)	320 ± 20	320 ± 20	310 ± 20	300 ± 20	300 ± 20
16NUS-07 (M3)	660 ± 30	640 ± 30	650 ± 30	630 ± 30	590 ± 30
16NUS-08 (M3)	540 ± 40	530 ± 40	530 ± 40	520 ± 30	480 ± 30
16NUS-09 (M3)	500 ± 20	490 ± 20	490 ± 20	480 ± 20	450 ± 20
16NUS-10 (M4)	1140 ± 80	1110 ± 70	1120 ± 80	1090 ± 70	1010 ± 70
16NUS-11 (M4)	1000 ± 50	970 ± 50	990 ± 50	960 ± 50	890 ± 50
16NUS-12 (M4)	570 ± 30	560 ± 30	570 ± 30	550 ± 30	510 ± 30
16NUS-13 (M4)	1090 ± 40	1050 ± 40	1070 ± 40	1040 ± 40	960 ± 30
16NUS-14 (M8)	4340 ± 100	4400 ± 100	4290 ± 100	4160 ± 90	4010 ± 90
16NUS-15 (M8)	117830 ± 1770	174050 ± 1810	168560 ± 1750	163540 ± 1690	158690 ± 1640
16NUS-16 (M8)	900 ± 30	880 ± 30	890 ± 30	870 ± 30	800 ± 30
16NUS-17 (M8)	1240 ± 60	1200 ± 60	1220 ± 60	1190 ± 60	1100 ± 50
16NUS-18 (M8)	1070 ± 50	1040 ± 50	1060 ± 50	1030 ± 50	950 ± 50
16NUS-19 (M8)	840 ± 30	810 ± 30	830 ± 30	810 ± 30	740 ± 30
16NUS-20 (M8)	870 ± 50	850 ± 50	860 ± 50	840 ± 50	770 ± 40
16NUS-21 (M9)	1350 ± 40	1310 ± 40	1330 ± 40	1290 ± 40	1200 ± 40
16NUS-22 (M9)	930 ± 60	900 ± 60	920 ± 60	890 ± 60	820 ± 50
16NUS-23 (M9)	870 ± 60	840 ± 60	860 ± 60	830 ± 60	770 ± 60
Deglaciation samples near Saqqap Tasersua					
16NUS-24	11270 ± 300	11420 ± 300	11120 ± 290	10805 ± 280	10430 ± 270
16NUS-27	8760 ± 350	8840 ± 350	8650 ± 840	8400 ± 330	8080 ± 320
Deglaciation samples near Pauiaivik Lake					
13GROR-66	10520 ± 180	10680 ± 180	10390 ± 170	10090 ± 170	9750 ± 160
13GROR-67	12210 ± 240	12410 ± 240	12050 ± 240	11710 ± 230	11340 ± 220
13GROR-68	11190 ± 220	11260 ± 220	11050 ± 210	10730 ± 210	10280 ± 200

^{10}Be ages are calculated using a sample density of 2.65 g cm^{-3} and an effective attenuation length of 160 g cm^{-2}. We assume negligible erosion over these timescales. All ^{10}Be concentrations are reported relative to 07KNSTD3110 with a reported ratio of 2.85 × 10^{-12} using a ^{10}Be half-life of 1.36 × 10^{6} years (Nishiizumi et al., 2007). Reported uncertainties are internal AMS uncertainties.

[a] Young et al. (2013b).

[b] Balco (2017).

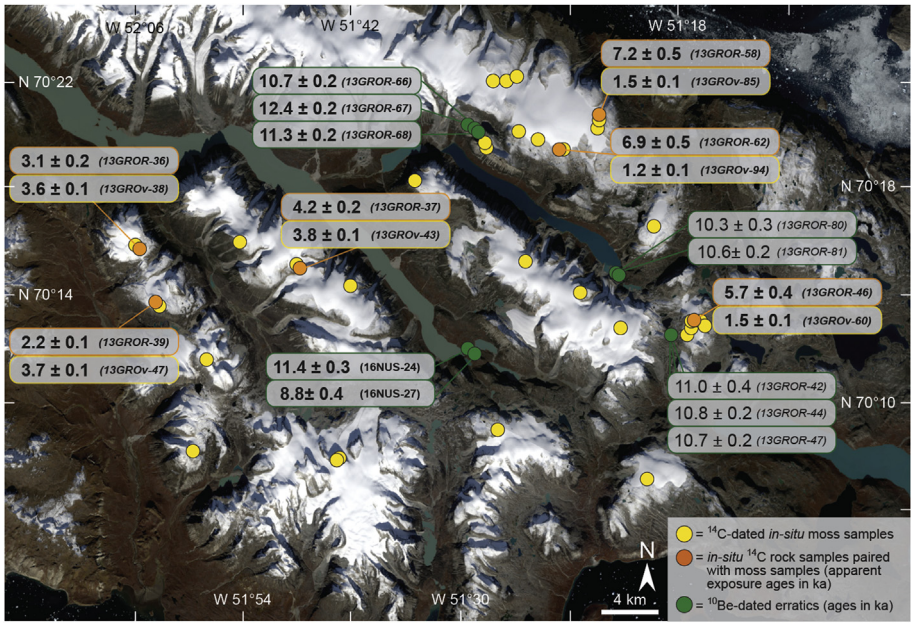

Fig. 5. Nuussuaq study area with cosmogenic exposure ages from this study (bold-face) and previous work. Yellow and orange circles indicate radiocarbon-dated *in situ* tundra moss samples (Schweinsberg et al., 2017) and apparent exposure ages from *in situ* ^{14}C bedrock samples (this study; ages in ka), respectively. Sample 13GROR-69 is located to the northwest on the island of Storøn (70.7°N, 51.8°W). ^{10}Be-dated perched boulders are also shown [green circles; this study and Schweinsberg et al. (2017)]. Base image is a Landsat8 natural color composite (RGB; 432) mosaic built with scenes acquired in August 2016. (For interpretation of the references to color in this figure legend, the reader is referred to the Web version of this article.)

Table 5
Apparent *in situ* ^{14}C exposure ages and pertinent sample information.

Sample ID	Latitude (°N)	Longitude (°W)	Elevation (m a.s.l.)	Thickness (cm)	[^{14}C][a] (10^5 atoms g^{-1})	Exposure age (LSD*n*)[b] (ka)	Exposure age (Lm)[b] (ka)
13GROR-36	70.2633	52.1152	1110	1.5	1.219 ± 0.040	3.1 ± 0.2	3.4 ± 0.2
13GROR-37	70.2519	51.8126	1249	3.0	1.625 ± 0.031	4.2 ± 0.2	4.6 ± 0.3
13GROR-39	70.2275	52.0629	1231	1.0	1.003 ± 0.042	2.2 ± 0.1	2.4 ± 0.2
13GROR-46	70.2157	51.0776	864	2.0	1.524 ± 0.056	5.7 ± 0.4	6.1 ± 0.5
13GROR-58	70.3495	51.2488	1051	5.0	2.037 ± 0.035	7.2 ± 0.5	7.8 ± 0.7
13GROR-62	70.3272	51.3151	1116	2.0	2.146 ± 0.057	6.9 ± 0.5	7.5 ± 0.7

[a] In situ ^{14}C concentrations using 10 g of sample. The following blank corrections have been subtracted from the total number of 14C atoms measured for given samples (prior to dividing by sample mass): 13GROR-36, -39, −46 = (1.54 ± 0.31) x 10^5 ^{14}C atoms; 13GROR-37, -58, −62 = (1.61 ± 0.12) x 10^5 ^{14}C atoms. AMS data reduction and standardization follows Hippe and Lifton (2014).

[b] Apparent *in situ* 14C exposure ages are relative to 2010, and calculated using CRONUS-Earth global time-integrated spallogenic production rate and LSDn scaling (13.0 ± 0.5 atoms g^{-1} yr^{-1}; Lifton et al., 2016; Borchers et al., 2016; Phillips et al., 2016; Balco et al., 2008; Balco, 2017), a topographic shielding correction of 1 (shielding was negligible at all sites), and a sample density of 2.65 g cm^{-3}. We assume zero erosion of these sample surfaces. The apparent *in situ* ^{14}C exposure ages are not corrected for time-dependent altitudinal changes associated with glacio-isostatic adjustment.

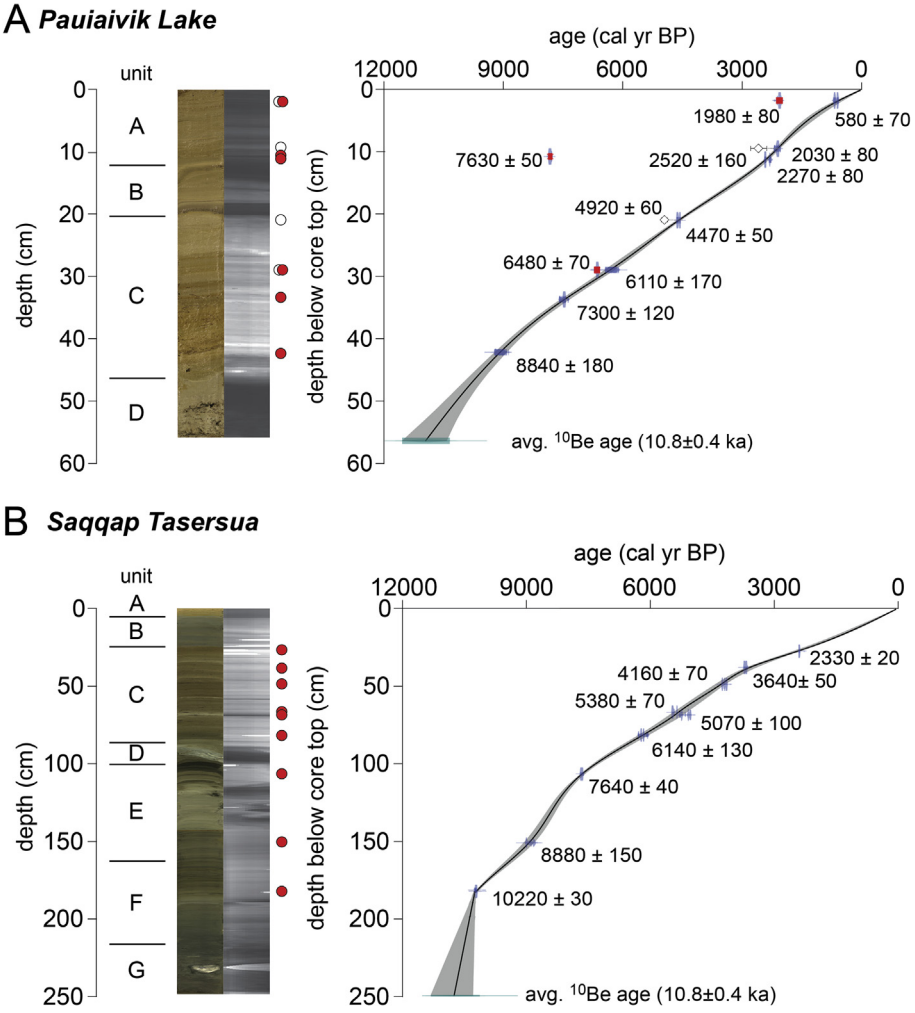

Fig. 6. Stratigraphy, x-radiographs, and age-depth relationships for proglacial lakes discussed in this study. A) Scanned image, x-radiograph, and age-depth model for 13PVK-A2. Radiocarbon sample locations are indicated by red and white circles for macrofossil and bulk sediment ages, respectively (Table 2). On the age-depth model plot, radiocarbon ages used in the model are shown in blue and the outliers are colored red. White diamonds indicate the uncorrected bulk sediment radiocarbon ages (Table 2). Light gray shading depicts 95% confidence intervals. Darker shades in the x-radiographs relate to denser material. Sedimentological units are indicated by letters A (top) through D (bottom); refer to the Supplemental File for descriptions. B) Age-depth model, core scan and x-radiograph for 16SAQ-B1. White sections in the x-radiograph of 16SAQ-B1 mark locations of radiocarbon samples taken prior to imaging. (For interpretation of the references to color in this figure legend, the reader is referred to the Web version of this article.)

Figs. S1, and S2), which are commonly used to reconstruct glacier size in lakes that have their mineral input dominated by glacial sources (e.g., Dahl et al., 2003). PCA highlights a closely tracking variability in the majority of parameters over the length of each lake sediment record. Many of these variations are aligned with independent proxies of climate and glacier change, thus supporting

the interpretation that PC1 scores can be used as a record of bedrock erosion (e.g., Balascio et al., 2015). Therefore, we infer the PC1 record to generally reflect changes in glacial activity and past fluctuations in GIC extent through time (Fig. 7; e.g., Balascio et al., 2015; Larsen et al., 2017; De Wet et al., 2017; Schweinsberg et al., 2017, 2018). However, we note that sediments in proglacial lakes can be the result of a complex set of physical processes (e.g., sediment storage, erosion and transport) as well as intra-lake processes (e.g., Dahl et al., 2003) that could impact the PC1 record.

5.2. ^{10}Be dating – perched boulders

Samples from perched boulder surfaces near Pauiaivik Lake ($n = 3$) gave ^{10}Be ages of 12.4 ± 0.2, 11.3 ± 0.2 and 10.7 ± 0.2 ka (Table 4). The average ^{10}Be age of these boulders is 11.0 ± 0.4 ka after excluding one old outlier (13GROR-67, 12.4 ± 0.2 ka), which may reflect inherited ^{10}Be inventories and is older than all other ^{10}Be ages, including previously published ^{10}Be ages of local deglaciation near Sikuiui Lake and outboard of the Uigorliup moraines (Fig. 1; ~10.7 ± 0.3 ka, Schweinsberg et al., 2017). Two boulders perched on bedrock near Saqqap Tasersua returned ^{10}Be ages of ~11.4 ± 0.3 and 8.8 ± 0.4 ka (Table 4). The ^{10}Be age of 11.4 ± 0.3 ka is in agreement with ^{10}Be ages of perched boulders near Pauiaivik Lake and other constraints for the local deglaciation of Nuussuaq (Cronauer et al., 2016; Schweinsberg et al., 2017). The other ^{10}Be age of 8.8 ± 0.4 ka (16NUS-27) is likely too young and considered an outlier. We interpret the average ^{10}Be age of 10.8 ± 0.4 ka [$n = 8$; this study and Schweinsberg et al. (2017)] to date the timing of deglaciation of eastern Nuussuaq.

5.3. Saqqap Tasersua moraines

Twenty-three ^{10}Be ages from boulders on ST moraine crests range from ~174 to 0.3 ka (Table 4; Fig. 8). This wide range of moraine boulder ages reflects a large degree of geologic scatter; certain ^{10}Be ages (16NUS-15, 174.1 ± 2.0 ka) are much too old when compared to the mean regional deglaciation age (~10.8 ± 0.4 ka), while other ^{10}Be ages are too young relative to the majority of ^{10}Be ages from the same moraine crest. Most of the ^{10}Be ages range from ~1.4 to 0.3 ka ($n = 19$), indicating that the ST moraines include crests that were deposited prior to and during the classic LIA interval.

We omit ^{10}Be ages from the ST moraines that are >2 ka ($n = 4$) from further discussion because these ages are significantly older than all other ^{10}Be ages in the population regardless of moraine position and likely reflect inherited ^{10}Be inventories. The innermost sampled moraine (M1) boulder ^{10}Be ages average 270 ± 20yr ($n = 3$; Table 4; Fig. 8). Boulders from M3 and M4 returned average ^{10}Be ages of 550 ± 80 ($n = 3$) and 1040 ± 70 yr ($n = 3$), respectively, after excluding one young outlier from each moraine position [16NUS-06 (M3) and 16NUS-12 (M4)]. We suggest that these two young outliers represent post-depositional disturbance, which likely occurred as these large, steep and previously ice-cored moraines stabilized during the past millennium (e.g., Crump et al.,

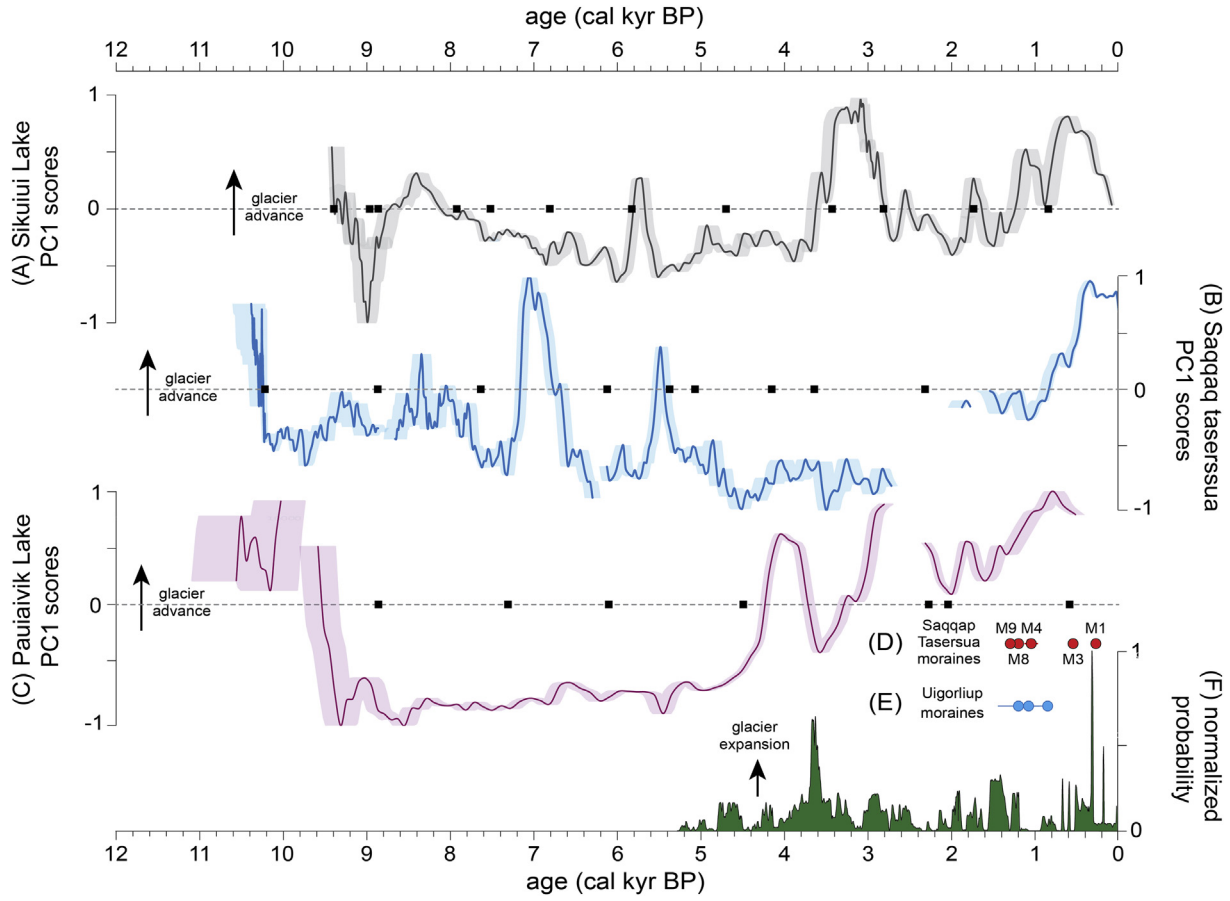

Fig. 7. Summary of glacier-size proxies from Nuussuaq during the Holocene. A) Sikuiui Lake PC1 scores (Schweinsberg et al., 2017). B) Saqqap Tasersua PC1 scores (this study). Black squares represent downcore radiocarbon ages. C) Pauiaivik lake PC1 scores (this study). D) Average ^{10}Be ages and uncertainties (red circles) for ST moraines. E) Mean ^{10}Be ages (blue circles) for the Uigorliup moraines (Young et al., 2015). F) West Greenland moss chronology ($n = 54$ samples; Schweinsberg et al., 2017). (For interpretation of the references to color in this figure legend, the reader is referred to the Web version of this article.)

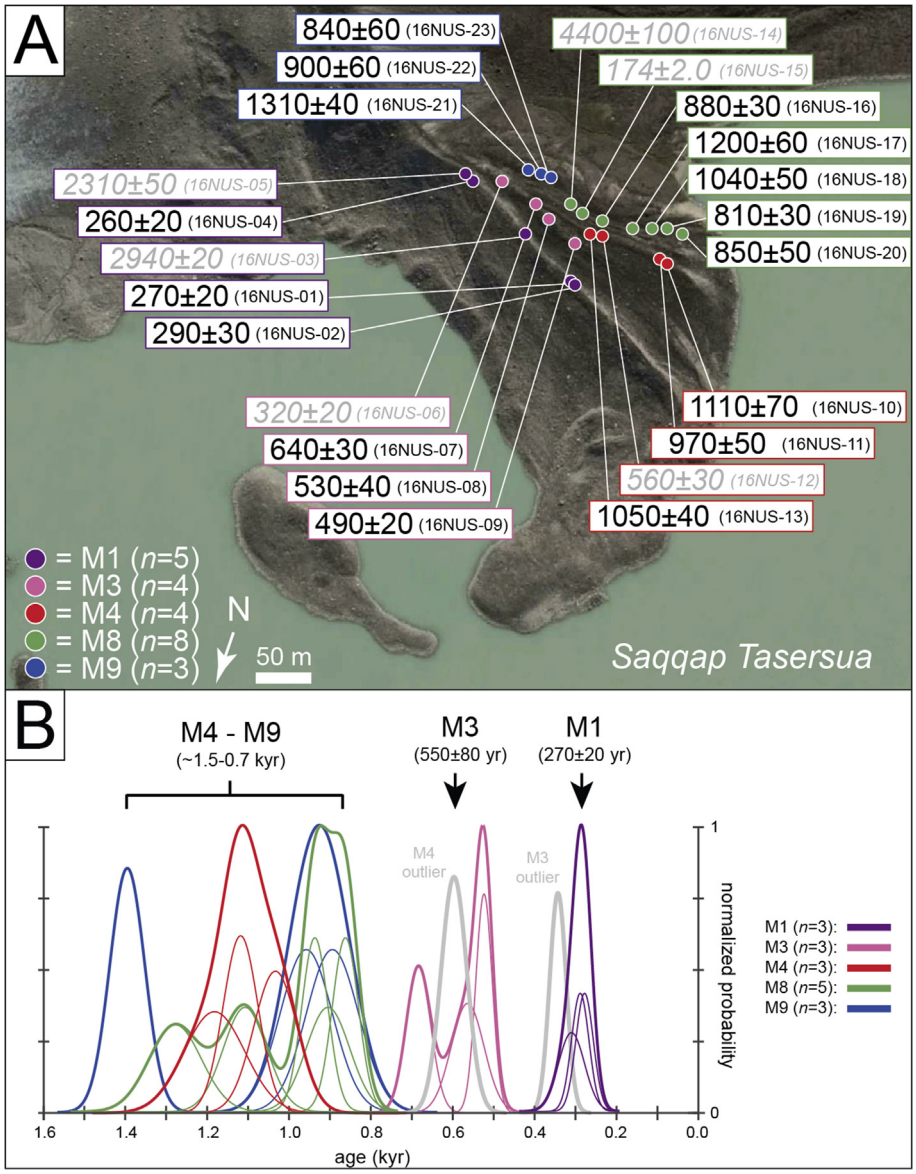

Fig. 8. Summary of ^{10}Be results from the ST moraines. A) Individual ^{10}Be ages and uncertainties expressed in years with the exception of 16NUS-15, which is in ka. Outliers are in gray italics. The modern glacier (2016 C.E.) is visible in the top left corner of the figure. Base image is from Google Earth. B) Normal kernel density estimates for all ^{10}Be ages less than 2 ka. There is significant overlap between ^{10}Be ages on M9, M8, and M4; most conservatively, the data indicate that these moraines were abandoned between ~1.5 and 0.7 ka.

2017).

The remaining ^{10}Be ages are from two moraine crests; five boulders are from M8, and three are from M9 (Fig. 8). Despite the stratigraphic position and distinct ridge morphology, ^{10}Be ages of moraine boulders from M9 overlap with ^{10}Be ages from M8 and M4. We propose three interpretations that may represent meaningful estimates for the true age of M4, M8 and M9 (Fig. 8 and Fig. S4), and point out that it is difficult to discern the true age for the outermost ST moraines due to the bimodal distribution of ^{10}Be ages from M8. Based on the morpho-stratigraphic relationship, M8 and M9 must be older than M4 (1040 ± 70 yr), suggesting that three samples (16NUS-16, 16NUS-19 and 16NUS-20) from M8 are too young. Averaging the remaining two ^{10}Be ages yields an average age of 1120 ± 110 yr for M8. Applying similar logic would suggest that samples 16NUS-22 and 16NUS-23 from M9 are also too young due to post-depositional disturbance, leaving the single ^{10}Be age of 1310 ± 40 yr to represent the best estimate for the age for M9 (Fig. S4).

Alternatively, averaging samples 16NUS-16, 16NUS-19, and 16NUS-20, which agree within uncertainties, yields an average ^{10}Be age of 850 ± 40 yr for M8, suggesting that three samples (16NUS-10, 16NUS-11, and 16NUS-13) from M4 are too old. Similarly, averaging the five ^{10}Be ages from both M8 and M9 that agree within 1σ uncertainty results in an average ^{10}Be age of 860 ± 40 yr for the outermost two moraines, yet suggests three samples from M4 (16NUS-10, 16NUS-11, and 16NUS-13) and one sample from M3 (16NUS-07) are outliers.

A third explanation is that M9 through M4 may have been built and subsequently abandoned by the glacier during a short time span, perhaps within a century. This could lead to a similar degree of geologic scatter between moraine positions that is a product of both inherited ^{10}Be inventories and post-depositional rotation. Thus, another possible and more conservative interpretation is that the valley glacier advanced and built M9 through M4 sometime between ~1.5 and 0.7 ka (Fig. 8B). Part of the scatter among ^{10}Be ages may be attributed to boulders that were first deposited on the

landscape following ice retreat from former (older) moraine positions, and then subsequently reincorporated into the glacier and deposited on a younger moraine at the culmination of a more recent glacier re-advance (Young et al., 2015).

5.4. *In situ* ^{14}C measurements and modeled exposure-burial scenarios

In situ ^{14}C in quartz from bedrock along six different ice cap margins yield apparent exposure ages ranging from ~7.2 to 2.2 ka (Table 5; Fig. 5). These relatively young exposure ages reflect varying burial by Holocene ice growth following deglaciation. To identify both the duration and timing of burial intervals at each particular site during the Holocene, *in situ* ^{14}C inventories are combined with radiocarbon ages of adjacent *in situ* moss samples reported by Schweinsberg et al. (2017). Possible exposure-burial histories for each moss-bedrock pair on Nuussuaq are presented in Fig. 9; each scenario is presented with three ice thickness scenarios (20, 35, and 100 m-thick ice cover). Operation IceBridge radar data reveal that ice caps on Nuussuaq are typically ~100 m thick, and tend to maintain a similar thickness to very near the ice cap margin where the bedrock and moss samples were collected. Thus, we suggest that the 100 m-thick scenarios are the most plausible, yet we present models with ice thicknesses of 20 and 35 m as sensitivity experiments.

Coupled *in situ* ^{14}C measurements and radiocarbon-dated moss at three sites on Nuussuaq are compatible with a period of continuous exposure following deglaciation followed by a period of ice cap occupation during the late Holocene that persisted until the sampling year (Fig. 9D–F). Exposure-burial modeling of samples 13GROR-37, 13GROR-58, and 13GROR-62 suggest that deglaciation of these sites occurred sometime between ~12.0 and 9.2 ka (Fig. 9D through 9F, 20 to 100 m-thick ice). Although somewhat variable, these model results are in agreement with ^{10}Be ages for local deglaciation from this study and previously published limits on the timing of deglaciation in eastern Nuussuaq (Roberts et al., 2013; O'Hara et al., 2017; Schweinsberg et al., 2017).

The remaining three sites with *in situ* ^{14}C measurements require an earlier period of burial in addition to a more recent interval of ice cover constrained by the *in situ* moss radiocarbon age when assuming deglaciation at ~10.8 ka (Fig. 9A–C). In addition to the most recent episode of burial, an additional ~940 years of 100 m-thick ice cover is necessary to cover sample site 13GROR-46 sometime earlier in the Holocene (Fig. 9C). Under thinner ice conditions (e.g., 20 m), the duration of this earlier burial interval is extended to ~1230 years for 13GROR-46. Although the timing of this earlier burial period is unknown, we suggest that the previous interval of 100 m-thick ice cover occurred sometime between ~3.7 and 2.7 ka based on the major episode of ice cap growth documented at ~3.7 ka in the regional moss dataset (Fig. 9C; Schweinsberg et al., 2017) and lake sediment records. Moreover, this timing is coincident with paired moss radiocarbon ages for three other sample sites (13GROR-36, 13GROR-37 and 13GROR-39) indicating that GIC growth occurred elsewhere on eastern Nuussuaq at this time.

Samples 13GROR-36 and 13GROR-39 were buried by recent ice cover longer than sample 13GROR-46, and therefore require a longer duration of earlier ice cover to match their respective ^{14}C inventories (Fig. 9A and B). If 13GROR-36 was shielded completely by 100 m-thick ice during burial intervals throughout the Holocene, the cumulative duration preceding the most recent interval of ice cover amounts to ~950 years. If ice thicknesses are reduced to 35 and 20 m during intervals of ice cover, an additional ~1160 and 1500 years of burial is necessary to meet the measured ^{14}C inventory, respectively.

The *in situ* ^{14}C inventory for sample 13GROR-39 is the lowest of all sites on Nuussuaq (Table 5, Fig. 9B), indicating that this site experienced the longest duration of burial since the onset of deglaciation. Ice must have covered the site for ~2100 (100 m) to 2500 (20 m) years in addition to continuous ice cover for the past ~3.7 ka (paired moss radiocarbon age) to match the measured *in situ* ^{14}C inventory. This results in a cumulative burial duration of 5.8–6.2 ka under ice thicknesses of 100 to 20 m, respectively. To account for this duration of burial, ice would have occupied the 13GROR-39 site earlier than the onset of Neoglaciation documented in the regional moss chronology at ~5 ka (e.g., Schweinsberg et al., 2017) and elsewhere in Greenland (e.g., Briner et al., 2016). We cannot rule out ice covering this specific site earlier than 5 ka; however, we note that this interval of prior burial, as well as the others required for samples 13GROR-36 and 13GROR-46, can be shifted later in the Holocene if local deglaciation occurred later at these localities.

6. Discussion

6.1. Early Holocene (11.7–8.3 ka)

Proglacial lake sediment records from Nuussuaq point to a dynamic glacial history with variable responses of local glaciers to Holocene climate changes (Fig. 7). Although the study lakes are close to one another (greatest distance is ~18 km; Fig. 1), variability exists in the lake sediment records and likely reflects a combination of other factors that modulate glacier fluctuations (e.g., hypsometry, valley gradient, debris cover), within-lake processes (e.g., redox conditions), and/or processes that govern sedimentation into glacier-fed lakes (e.g., catchment size, mass wasting events, paraglacial sediment remobilization). Despite some differences between our glacier-size reconstructions, we also find similarities between the lake sediment records; however, our interpretations are less certain prior to ~5 cal ka BP when the regional moss and moraine chronologies are absent (Fig. 7; Young et al., 2015; Schweinsberg et al., 2017).

Following deglaciation of eastern Nuussuaq ~10.8 ka, GIC decreased in size in response to peak values in summer insolation (Fig. 10; Berger and Loutre, 1991). However, the Nákâgajoq mountain moraines, dated to ~10.6 ka, suggest that some local glaciers on Nuussuaq experienced an advance/stillstand soon after the retreat of the GrIS (Figs. 1 and 10; O'Hara et al., 2017). Multiple studies of GIC and GrIS margin change along the West Greenland coastline have proposed a link between early Holocene freshwater forcing and associated cooling with glacier and GrIS margin behavior (e.g., Alley and Ágústsdóttir, 2005; Young et al., 2013a; O'Hara et al., 2017; Schweinsberg et al., 2017, 2018; Lesnek and Briner, 2018). It is suggested that the advance/stillstand of local glaciers that led to the formation of the Nákâgajoq mountain moraines may be due to regional cooling associated with the repeated release of Laurentide Ice Sheet (LIS) meltwater into the North Atlantic Ocean during the early Holocene (O'Hara et al., 2017).

6.2. Middle Holocene (~8.3–4.3 ka)

Saqqap Tasersua PC1 scores show a low-amplitude yet sharp increase at ~8.3 cal ka BP that occurs within an interval of elevated PC1 scores from Sikuiui Lake between ~8.8 and 8.0 cal ka BP (Fig. 7). The elevated PC1 scores in both lake sediment records may reflect a brief glacier re-advance that relates to the '8.2 event,' a ~150-yr cooling episode that is similarly thought to have been triggered by an LIS outburst flood (Alley et al., 1997; Rasmussen et al., 2007). We note that the correlation of increased Nuussuaq GIC activity with the 8.2 event is somewhat speculative, as our records are consistent

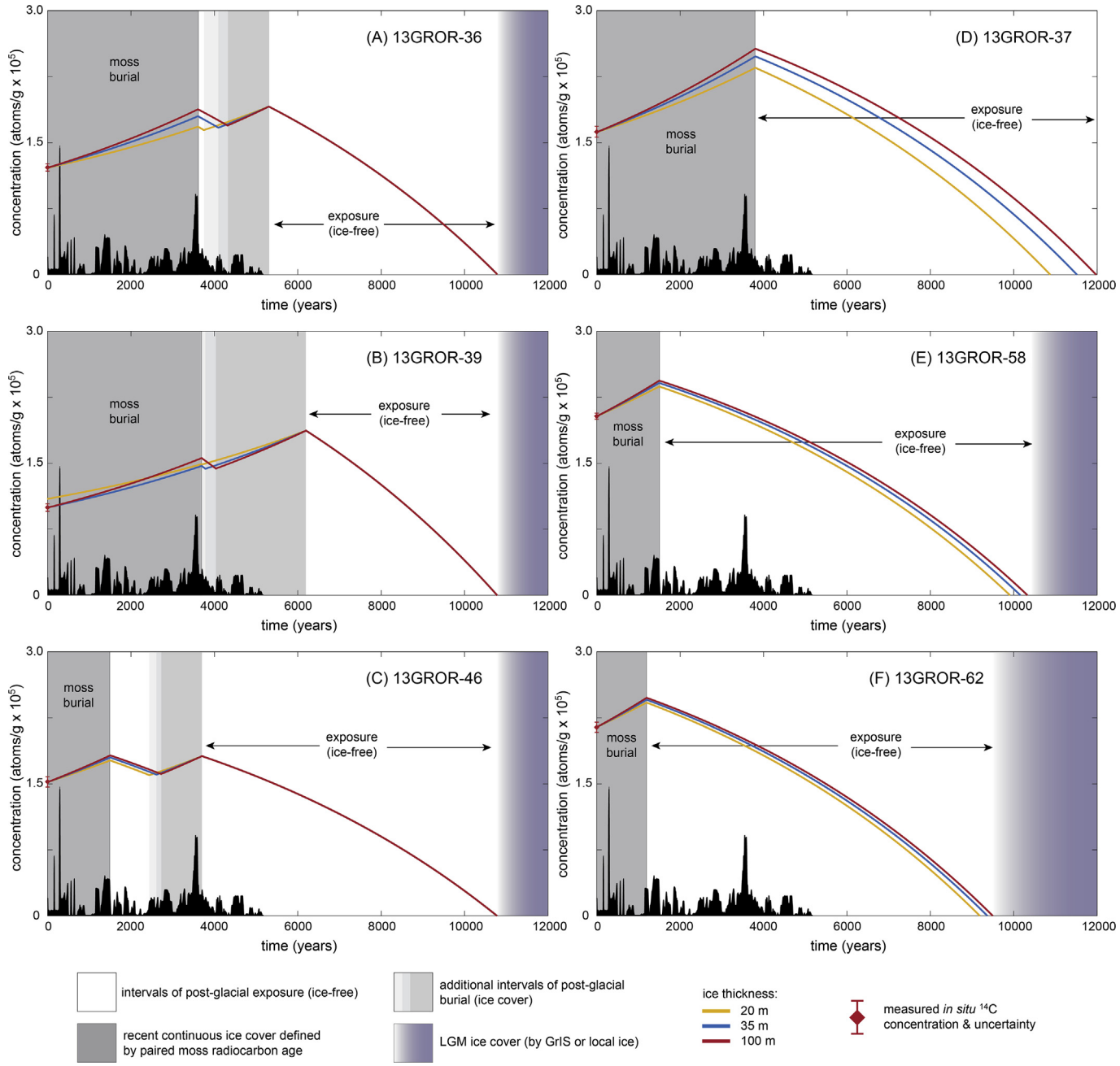

Fig. 9. Modeled exposure-burial histories for Nuussuaq sample sites. Aggregated PDF represents the West Greenland moss dataset (Schweinsberg et al., 2017). Differences in the duration of earlier burial episodes is a function of ice thickness.

with only one of a number of proposed LIS discharge events during the early Holocene (Fig. 10; Jennings et al., 2015). However, evidence for this relationship is found for other GIC and GrIS margin changes in the Baffin Bay region (e.g., Young et al., 2013a; Balascio et al., 2015; Schweinsberg et al., 2018; Lesnek and Briner, 2018). Collectively, these studies support hypotheses that LIS freshwater input and the associated changes in oceanic circulation acted as a primary forcing mechanism for early and middle Holocene GIC and GrIS margin fluctuations around Greenland. It is also plausible that early and middle Holocene glacier fluctuations on Nuussuaq were influenced by other climate forcings unrelated to freshwater forcing. For example, large and frequent volcanic eruptions may have triggered summer cooling and subsequently affected ocean surface conditions and sea-ice formation throughout the Holocene, and may have led to intervals of positive glacier mass balance (Fig. 10; Kobashi et al., 2017).

In contrast to the Sikuiui Lake reconstruction, the Pauiaivik Lake record suggests there was little to no glacier ice in the catchment between ~9.5 and 4.3 cal ka BP (Figs. 7 and 10). This interpretation is based on the MS and density data and PC1 scores, which are the lowest of the record and show reduced variability during this interval, relative to the deglacial sediments and the mineral-rich sediments throughout the last ~4.3 cal ka BP (Fig. S1). This interval is also marked by high LOI values (~35–9%) suggesting that this period was accompanied by an increase in primary productivity due to a lack of mineral-rich sediment input (e.g., glacial flour).

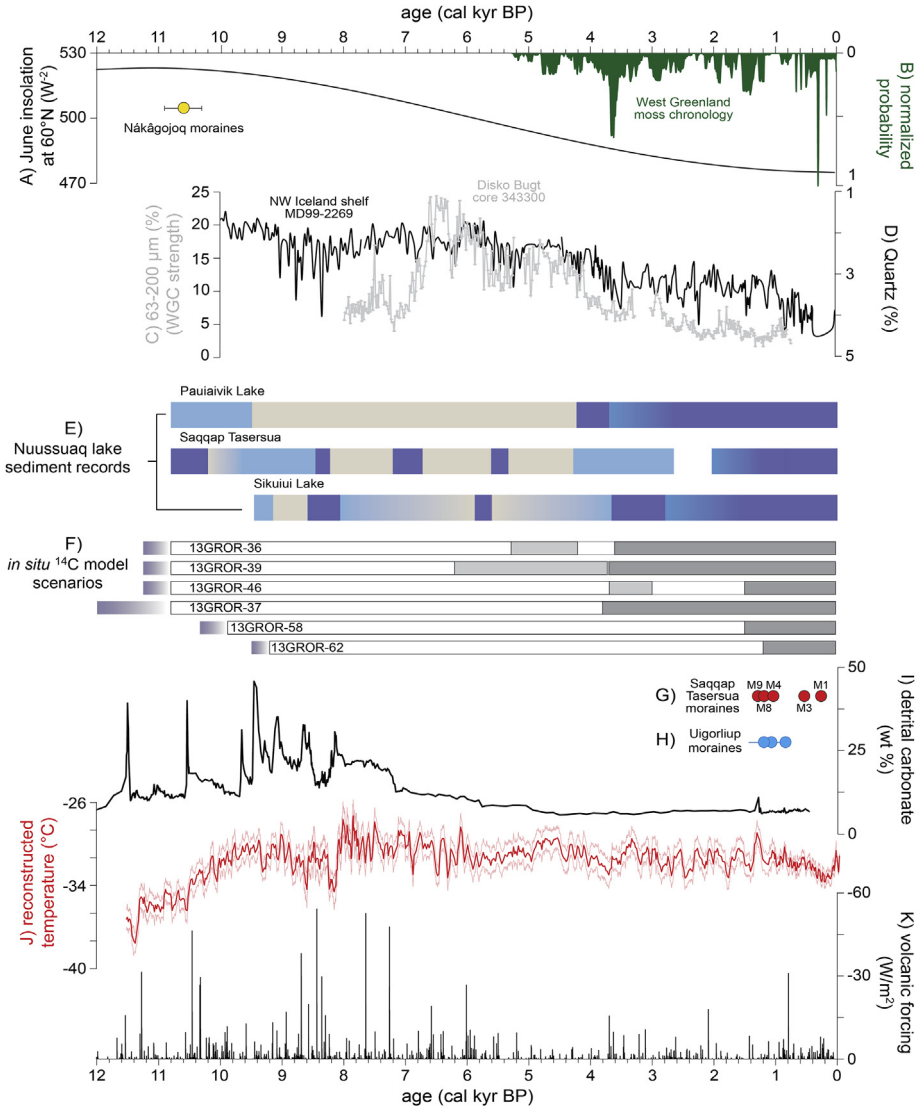

Fig. 10. Glacier-size reconstructions from Nuussuaq compared with potential climate forcings during the Holocene. A) June insolation at 60 °N (Berger and Loutre, 1991); B) Aggregated distributions of radiocarbon ages of mosses from West Greenland ($n = 54$, green curve; Schweinsberg et al., 2017); C) West Greenland Current strength proxy from core 343300 (cruise MSM05/03 of the R/V *Maria S. Merlan*), Disko Bugt, West Greenland (sand content [% fraction 63–200 µm); Perner et al. (2013); D) Drift ice proxy record (% quartz) from core MD99–2269 (IMAGES V cruise, Leg 3, to the Nordic Seas), northwest Iceland (Moros et al., 2006). E) Proglacial lake sediment records from Nuussuaq (this study and Schweinsberg et al., 2017). Light blue boxes represent periods of glacial activity (darker blue = enhanced glacier activity), tan boxes suggest no glacier was present in the catchment and/or glacial activity was reduced. F) The timing and duration of ice-free periods (open rectangles) and episodes of ice cover (gray boxes; darker gray = ice cover defined by paired moss sample) estimated by the modeled *in situ* ^{14}C scenarios. Purple shaded bars reflect LGM ice cover. G) Average ^{10}Be ages of the ST moraines (this study); H) Mean ages (blue circles) of the Uigorliup moraines (Young et al., 2015); I) Detrital carbonate content of marine sediment core MD99-2236 from the Labrador Shelf (Jennings et al., 2015). J) GISP2 temperature (red line) with 2σ error (Kobashi et al., 2017). K) Volcanic forcing generated from sulfate concentrations in GISP2 (Kobashi et al., 2017). (For interpretation of the references to color in this figure legend, the reader is referred to the Web version of this article.)

PC1 scores from Saqqap Tasersua and Sikuiui Lake are variable during the middle Holocene, yet imply an overall reduction in glacier size from ~8 cal ka BP until ~4.5 and 3.8 cal ka BP, respectively (Fig. 7; Schweinsberg et al., 2017). Two exceptions to this pattern of reduced glacier size include an interval of mineral-rich sediment input that punctuates the Saqqap Tasersua sediment record at ~7 cal ka BP, and an abrupt peak in PC1 scores registered in both the Sikuiui Lake and Saqqap Tasersua PC1 records between ~5.9 and 5.3 cal ka BP (Figs. 6 and 7). Although the distinct excursion in PC1 scores and downcore proxy data at ~7 cal ka BP in the Saqqap Tasersua sediment record is not reflected in the other Nuussuaq glacier-size reconstructions, the sedimentological characteristics of the unit (e.g., no visible grading, clayey silt) do not suggest evidence for a mass-wasting event. We postulate that because Saqqap Tasersua is fed by multiple ice-cap outlet glaciers, this excursion in PC1 scores may reflect an integrated signal of increased glacier size within the catchment. Alternatively, surge-type glaciers may be responsible for the excursion in PC1 scores; however, surging glaciers are far less common in eastern Nuussuaq relative to the volcanic bedrock terrain of western Nuussuaq (Citterio et al., 2010).

At present, there is a single meltwater source to Pauiaivik Lake while Sikuiui Lake receives meltwater from two separate ice caps (Figs. 1 and 2). Thus, it is possible that one or more of the ice-cap outlet glaciers that transports glacigenic sediments to Saqqap Tasersua experienced a re-advance at a time when glaciers supplying meltwater to the other study lakes were not sufficiently active to produce a signal in the sediment record. Alternatively,

each study lake may exhibit a different sensitivity to up-valley glacier changes, which may account for differences between the PC1 scores and glacier-size reconstructions. For example, if the ice cap margin near Pauiaivik Lake never drained into the lake during the middle Holocene as suggested by Pauiaivik Lake sediment record (Fig. 7), sedimentological evidence of glacier fluctuations during this interval would not be captured in the 13PVK-A2 sediment core. Although rarely documented, records of GIC advances during the early to middle Holocene have been noted elsewhere in Greenland (Fig. S5). A similar excursion in PC1 scores and a concomitant decrease in LOI values is recorded at ~7.2 and 6.2 ka in southeast Greenland (Kulusuk Lake), but are interpreted as sediment influxes from paraglacial processes (Balascio et al., 2015). Local glacier moraines have also been dated to between ~9.6 and 6.3 ka and between 5.5 and 5.0 ka in North Greenland (Möller et al., 2010).

A second excursion in the Sikuiui Lake PC1 scores occurs at ~5.7 cal ka BP and corresponds to a thin mineral-rich silt layer that is interpreted as a minor glacial re-advance (Schweinsberg et al., 2017). A peak of comparable amplitude, timing, and duration is documented in the Saqqap Tasersua PC1 record, and is associated with a fine-grained silt layer that interrupts organic-rich sediments in this portion of the core. We interpret these changes in sedimentology as a brief glacier advance between ~5.9 and 5.3 cal ka BP due to the similar characteristics of this event captured in two lake sediment records (Fig. 7). We acknowledge that a small offset in timing exists between the two sediment records; this offset may be due to chronological uncertainties and/or reflect lag time between the different glacier systems due to non-climatic effects. This brief GIC advance between ~5.9 and 5.3 ka occurs just after a period of sustained volcanic activity at ~6.0 ka and a decrease in reconstructed Greenland temperatures (Fig. 10; Kobashi et al., 2017). Similarly, an abrupt reduction in Greenland temperature coincides with the possible glacier advance at ~7 ka recorded in the Saqqap Tasersua sediments, and follows several of the largest volcanic eruptions documented in the early Holocene (Kobashi et al., 2017). This increase in glacier activity on Nuussuaq may also correlate with advances of local glaciers in southwest Greenland from ~5.5 to 4.1 cal ka BP, pointing to a regional response of local glaciers along the West Greenland coastline to a common climate forcing (Fig. S5; Larsen et al., 2017). Returning to the in-situ ^{14}C measurement from GROR-39, there is some evidence from these lake sediment records for potential middle Holocene ice expansion phases.

6.3. Late Holocene (~4.3 ka to present)

6.3.1. Onset of Neoglaciation (~4.3–2 ka)

Our glacier-size reconstructions suggest that GIC expanded between ~4.3 and 2 ka on Nuussuaq shortly following the earliest evidence of snowline depression and ice cap expansion documented in the *in situ* moss chronology (Figs. 7 and 10; Schweinsberg et al., 2017). The earliest evidence of glacier expansion documented in our sediment records occurred in the Pauiaivik Lake catchment at ~4.3 cal ka BP following several millennia with reduced glacier size. This transition is marked by an abrupt increase in mineral-rich input at ~4.3 cal ka BP, and may be correlative to a low-amplitude rise in PC1 scores (increased glacier size) in the Saqqap Tasersua lake sediment record. It is difficult to identify the onset of late Holocene GIC growth in the Saqqap Tasersua record due to the data gap in the downcore proxy data; however, the PC1 values before and after the data gap suggest net glacier expansion began sometime between ~3 and 2 ka (Fig. 7). Similar to Pauiaivik Lake, the shift from relatively reduced GIC size to increased glacier growth is abrupt in the Sikuiui Lake PC1 record from 4.0 to 3.5 ka, and closely follows widespread ice expansion inferred from the *in situ* moss dataset (Schweinsberg et al., 2017). An interval of increased GIC activity is similarly recorded in the Pauiaivik Lake PC1 record beginning ~3.6 ka, but is more gradual relative to the abrupt transition documented in the Sikuiui Lake PC1 scores (Fig. 7).

The abundant geological evidence that reveals glacier expansion between ~4.0 and 3.5 ka around the Northern Hemisphere points to hemispheric-wide climate forcing(s) driving centennial-scale glacier variability (e.g., Solomina et al., 2015). Some studies of GIC behavior around the North Atlantic region have suggested that intervals of snowline depression and increased glacier activity may be attributed to changes in oceanic circulation patterns (e.g., Geirsdóttir et al., 2013; Larsen et al., 2013; Balascio et al., 2015; Schweinsberg et al., 2017). Marine records from around West Greenland document decreases in West Greenland Current strength in the mid-to-late Holocene, which may have played a role in the transition to colder terrestrial conditions and subsequent glacier expansion (Fig. 10; e.g., Perner et al., 2013; Moros et al., 2016 and references therein). Alternatively, intervals of explosive volcanism may have affected past climate on multidecadal timescales and led to conditions favorable for GIC expansion (Fig. 10; Kobashi et al., 2017). Intervals of sustained volcanic activity have been proposed to exert a strong influence on centennial to millennial-scale temperature change throughout the Holocene in Greenland, implying that volcanic impacts may have been prevalent throughout the Holocene in this region (Fig. 10; Kobashi et al., 2017).

6.3.2. Latest Neoglacial (~2 ka to present)

Our proglacial lake sediment glacier-size reconstructions reveal that GIC on Nuussuaq successively advanced during the late Holocene before the onset of the LIA period (Fig. 7). The primary intervals of GIC growth occurred at ~1.8, 1.2, 0.7 and 0.4 cal ka BP, and are broadly synchronous with other late Holocene GIC records around Greenland (Fig. S5). For example, radiocarbon ages of *in situ* mosses and a lake sediment reconstruction near Sukkertoppen Iskappe register episodes of GIC growth at ~1.8, 1.2 and 0.7 ka (Schweinsberg et al., 2018) that are coeval with the timing of GIC fluctuations on Nuussuaq. In Southeast and Southwest Greenland, lake sediment archives reveal that local glaciers advanced at ~1.4 and 1.6 ka, respectively (Fig. S5; Balascio et al., 2015; Larsen et al., 2017), and in East Greenland, the Bregne Ice Cap advanced at ~1.9 ka (Lowell et al., 2013; Levy et al., 2014).

The ^{10}Be moraine chronology for the ST moraine complex provides additional support for extensive glaciers prior to the LIA interval in this region of the Arctic. The innermost ST moraines, M3 and M1, date to ~1470 and 1750 C.E., respectively, and confirm that mountain glaciers on Nuussuaq increased in size within the classic LIA interval (Figs. 8 and 10). However, the ^{10}Be ages of the outermost ST moraines, M9 through M4, date between ~520 and 1320 C.E., and reveal that some glaciers on Nuussuaq reached a larger extent centuries prior to the LIA maximum and during the European MWP. The Uigorliup (dated to ~1160 C.E.; Young et al., 2015) and ST moraines record extensive ice, but minor net retreat, during this time interval. Furthermore, ^{10}Be ages for both Nuussuaq moraine sequences date between radiocarbon age clusters of *in situ* moss at ~1.4 ka and the LIA, supporting the interpretation that gaps in the moss chronology may reflect minor ice margin recession following an earlier ice advance (Schweinsberg et al., 2017).

The Nuussuaq moraine chronologies support other ^{10}Be and ^{36}Cl-dated local glacier moraine sequences in the Baffin Bay region that point to the extensive build-up of ice during the latest Holocene. Local glacier moraines in Naqsaq valley, Baffin Island, date between ~1070 and 1700 C.E. ($n = 19$), suggesting that Naqsaq glacier reached a position similar to its LIA extent as early as ~1070

C.E. (Young et al., 2015). Similarly, moraines in Ayr Lake valley, Baffin Island, date to ~1240 C.E. ($n = 3$; Young et al., 2015), and moraines fronting Lyngmarksbræen on Disko island date to ~1200 C.E. ("M2" of Jomelli et al., 2016). Collectively, these results imply that at least four individual ice caps in the Baffin Bay region experienced near-synchronous glacier culminations before the LIA (Young et al., 2015; Jomelli et al., 2016).

The preservation of late Holocene moraine sequences in the Baffin Bay region are often controlled by local topography; most late Holocene moraines are found on the uphill side of the main valley floor. Thus, it is likely that late Holocene moraines existed in other glacier forefields but were subsequently overrun by the most recent glacier advance (Young et al., 2015). It has been questioned whether the topography conducive to late Holocene moraine preservation may cause the outlet glaciers depositing these moraines to be relatively insensitive to modest changes in equilibrium-line altitude (Pendleton et al., 2017). We support caution in interpreting regional climatic patterns from individual records; however, our other glacier-size proxies and previously published regional glacier chronologies provide additional evidence for net glacier growth throughout the latest Holocene (Young et al., 2015; Schweinsberg et al., 2017). An emerging array of evidence points to extended glaciers prior to the local LIA culmination on Nuussuaq and around Baffin Bay, implying that relatively larger glaciers spanning the past ~1200 years may be a coherent regional signature of late Holocene glacier activity of the northwestern North Atlantic (Young et al., 2015; Jomelli et al., 2016).

Our glacier-size proxies from eastern Nuussuaq support a potential link to anti-phase centennial-scale climate variability between northwestern Europe and the Baffin Bay region during the latest Holocene (e.g., Winsor et al., 2014; Young et al., 2015). Young et al. (2015) proposed that a persistent positive state of the North Atlantic Oscillation (NAO^+) may have led to a relatively cold climate around Baffin Bay and relatively warmer temperatures in Europe. Contemporary glacier studies also identify a climatic dipole across Greenland, and suggest that during a sustained phase of NAO^+ there are colder and drier conditions in West Greenland and increased precipitation associated with warmer conditions in East Greenland (Bjørk et al., 2018), further suggesting that the primary driver of GIC change in the Baffin Bay is summer temperature (e.g., Miller et al., 2012; Young et al., 2015). In addition to internal modes of atmospheric variability, it is likely that ocean-atmosphere-sea ice interactions or volcanic and/or solar forcing influenced Nuussuaq GIC changes (Moreno-Chamarro et al., 2016; Jomelli et al., 2016). Several recent studies have identified solar and volcanic forcing, and concomitant positive sea-ice feedbacks, as important triggers for centennial-scale climate change (e.g., Sigl et al., 2015; Swingedouw et al., 2015; Miller et al., 2012).

7. Conclusions

Using multiple independent reconstructions, we present a continuous high-resolution record of GIC change on eastern Nuussuaq, West Greenland, spanning the past ~10.8 ka. The observed pattern of GIC fluctuations on Nuussuaq is consistent with the broad picture of Holocene glacier oscillations documented elsewhere in Greenland and the Northern Hemisphere (e.g., Solomina et al., 2015, 2016). Coupled with previously published age constraints from Nuussuaq (Roberts et al., 2013; O'Hara et al., 2017; Schweinsberg et al., 2017), our results support a timing of local deglaciation between ~11.0 and 10.5 ka. Our data reveal that Nuussuaq glaciers may have been sensitive to regional-scale oceanographic changes in the early Holocene that were most likely influenced by freshwater injections into the North Atlantic Ocean (e.g., Alley et al., 1997; Alley and Ágústsdóttir, 2005; Jennings et al., 2015) as well as volcanic perturbations and the associated reduction in atmospheric temperatures on Greenland (Kobashi et al., 2017).

Despite an overall reduction in GIC size during the regional HTM (e.g., Briner et al., 2016), Nuussuaq glaciers may have briefly advanced at ~7 ka and between ~5.9 and 5.3 ka. Glacier growth at this time in the Arctic is poorly documented, and we note that additional glacier reconstructions spanning the early to middle Holocene are required to thoroughly assess whether glacier advances during this interval constitute a regional signature of GIC variability in West Greenland.

Our records reveal asynchronous regrowth of GIC between ~4.3 and 2 ka emphasizing the variable responses of individual glaciers to late Holocene climate changes on Nuussuaq. The subsequent millennia were characterized by gradually increasing glacier size in accordance with gradual declining summer insolation. Superimposed on the progressive increase in glacier growth are frequent, high-amplitude GIC fluctuations throughout the late Holocene; the most significant periods of GIC expansion occurred at ~3.7 and 2.8 ka, and throughout the past ~2 ka. The ^{10}Be chronology of the ST moraine sequence combined with nearby glacier chronologies (Young et al., 2015; Jomelli et al., 2016; Schweinsberg et al., 2017) suggest that Nuussuaq glaciers, and some other glaciers fringing Baffin Bay, experienced several culminations during the past millennium.

It remains difficult to identify the primary climate forcing mechanisms driving late Holocene local glacier variability in Greenland due to the scarcity of continuous and/or well-dated records documenting local glacier extents. We find that our glacier-size proxy records from Nuussuaq during the middle to late Holocene are broadly consistent with relatively lower reconstructed Greenland summer air temperatures and occur during or following intervals of volcanic perturbations (Kobashi et al., 2017). However, our glacier reconstructions are also in step with marked changes in regional oceanic circulation patterns during the late Holocene. While more research on alpine glacier change would help confirm the climate forcings postulated here, this study provides new records of GIC fluctuations that may help discern the complex structure of Holocene climate changes, and aid in examining the timing, expression, and magnitude of glacier response to Holocene climate change in the northwestern North Atlantic.

Acknowledgements

The authors thank Casey Beel for field assistance and Alia Lesnek and Christopher Sbarra for assistance in the laboratory. CH2M Hill Polar Field Services provided logistical support. This work was supported by the National Geographic Society (Grant 9796) and a National Science Foundation grant (ARC-1204005). This is LLNL-JRNL-760292 and LDEO publication #8318.

Appendix A. Supplementary data

Supplementary data to this article can be found online at https://doi.org/10.1016/j.quascirev.2019.05.007.

References

Alley, R.B., Ágústsdóttir, A.M., 2005. The 8k event: cause and consequences of a major Holocene abrupt climate change. Quat. Sci. Rev. 24, 1123–1149.
Alley, R.B., Mayweski, P.A., Sowers, T., Stuiver, M., Taylor, K.C., Clark, P.U., 1997. Holocene climatic instability: a prominent, widespread event 8200 yr ago. Geology 25, 483–486.
Axford, Y., Briner, J.P., Miller, G.H., Francis, D.R., 2009. Paleoecological evidence for abrupt cold reversals during peak Holocene warmth on Baffin Island, Arctic Canada. Quat. Res. 71, 142–149.
Badding, M.E., Briner, J.P., Kaufman, D.S., 2013. ^{10}Be ages of late Pleistocene

deglaciation and Neoglaciation in the North-central brooks range, Arctic Alaska. J. Quat. Sci. 28, 95–102.
Balascio, N.L., D'Andrea, W.J., Bradley, R.S., 2015. glacier response to North Atlantic climate variability during the Holocene. Clim. Past 11, 1587–1598.
Balco, G., 2017. Production rate calculations for cosmic-ray-muon-produced ^{10}Be and ^{26}Al benchmarked against geological calibration data. Quat. Geochronol. 39, 150–173.
Balco, G., Stone, J.O., Lifton, N.A., Dunai, T.J., 2008. A complete and easily accessible means of calculating surface exposure ages or erosion rates from 10Be and 26Al measurements. Quat. Geochronol. 3, 174–195.
Bakke, J., Trachsel, M., Kvisvik, B.C., Nesje, A., Lysså, A., 2013. Numerical analyses of a multi proxy data set from a distal glacier-fed lake, Sørsendalsvatn, western Norway. Quat. Sci. Rev. 73, 182–195.
Barclay, D.J., Wiles, G.C., Calkin, P.E., 2009. Holocene glacier fluctuations in Alaska. Quat. Sci. Rev. 28, 2034–2048.
Beel, C.R., Lifton, N.A., Briner, J.P., Goehring, B.M., 2016. Quaternary evolution and ice sheet history of contrasting landscapes in Uummannaq and Sukkertoppen, western Quaternary, Greenland. Quat. Sci. Rev. 149, 248–258.
Bennike, O., 2000. Palaeoecological studies of Holocene lake sediments from west Greenland. Palaeogeography. Palaeogeogr. Palaeoclimatol. Palaeoecol. 155, 285–304.
Bennike, O., Anderson, N.J., McGowan, S., 2010. Holocene palaeoecology of south-west Greenland inferred from macrofossils in sediments of an oligosaline lake. J. Paleolimnol. 43, 787–798.
Berger, A., Loutre, M.F., 1991. Insolation values for the climate of the last 10 million years. Quat. Sci. Rev. 10, 297–317.
Blaauw, M., 2010. Methods and code for 'classical' age-modelling of radiocarbon sequences. Quat. Geochronol. 5, 512–518.
Bjørk, A.A., Aagaard, S., Lutt, A., Khan, S.A., Box, J.E., Kjeldsen, K.K., Larsen, N.K., Korsgaard, J.J., Cappelen, J., Colgan, W.T., Machguth, H., Andresen, C.S., Peings, Y., Kjær, K.H., 2018. Changes in Greenland's peripheral glaciers linked to the North Atlantic Oscillation. Nat. Clim. Change 8, 48–52.
Boldt, B.R., Kaufman, D.S., McKay, N.P., Briner, J.P., 2015. Holocene summer temperature reconstruction from sedimentary chlorophyll content, with treatment of age uncertainties, Kurupa Lake, Arctic Alaska. The Holocene 25, 641–650.
Borchers, B., Marrero, S., Balco, G., Caffee, M., Goehring, B., Lifton, N., Nishiizumi, K., Phillips, F., Schaefer, J., Stone, J., 2016. Geological calibration of spallation production rates in the CRONUS-Earth project. Quat. Geochronol. 31, 188–198.
Briner, J.P., McKay, N.P., Axford, Y., Bennike, O., Bradley, R.S., de Vernal, A., Fisher, D., Francus, P., Fréchette, B., Gajewski, K., Jennings, A., Kaufman, D.S., Miller, G., Rouston, C., Wagner, B., 2016. Holocene climate change in Arctic Canada and Greenland. Quat. Sci. Rev. 147, 340–364.
Citterio, M., Paul, F., Ahlstrøm, A.P., Jepsen, H.F., Weidick, A., 2010. Remote sensing of glacier change in West Greenland: accounting for the occurrence of surge-type glaciers. Ann. Glaciol. 50, 70–80.
Clague, J.J., Koch, J., Geertsema, M., 2010. Expansion of outlet glaciers of the Juneau Icefield in northwest British Columbia during the past two millennia. The Holocene 20, 447–461.
Clark, P.U., Dyke, A.S., Shakun, J.D., Carlson, A.E., Clark, J., Wohlfarth, B., Mitrovica, J.X., Hostetler, S.W., McCabe, A.M., 2009. The last glacial maximum. Science 325, 710–714.
Corbett, L.B., Bierman, P.R., Rood, D.H., 2016. An approach for optimizing *in situ* cosmogenic ^{10}Be sample preparation. Quat. Geochronol. 33, 24–34.
Cronauer, S.L., Briner, J.P., Kelley, S.E., Zimmerman, S.R.H., Morlighem, M., 2016. ^{10}Be dating reveals early-Holocene age of the Drygalski Moraines in central West Greenland. Quat. Sci. Rev. 147, 59–68.
Crump, S.E., Anderson, L.S., Miller, G.H., Anderson, R.S., 2017. Interpreting exposure ages from ice-cored moraines: a Neoglacial case study on Baffin Island, Arctic Canada. J. Quat. Sci. 32, 1049–1062.
Dahl, S.O., Bakke, J., Lie, Ø., Nesje, A., 2003. Reconstruction of former glacier equilibrium-line altitudes based on proglacial sites: an evaluation of approaches and selection of sites. Quat. Sci. Rev. 22, 275–287.
Davis, P.T., Menounos, B., Osborn, G., 2009. Holocene and latest Pleistocene alpine glacier fluctuations: a global perspective. Quat. Sci. Rev. 28, 2021–2033.
De Wet, G.A., Balascio, N.L., D'Andrea, W.J., Bakke, J., Bradley, R.S., Perren, B., 2017. Holocene glacier activity reconstructed from proglacial lake Gjøavatnet on Amsterdamøya, Svalbard. Quat. Sci. Rev. 1–16.
Falconer, G., 1966. Preservation of vegetation and patterned ground under a thin ice body in northern Baffin Island, northern Baffin Island, N.W.T. Geogr. Bull. 8, 194–200.
Farnsworth, L.B., Kelly, M.A., Bromley, G.R., Axford, Y., Osterberg, E.C., Howley, J.A., Jackson, M.S., Zimmerman, S.R., 2018. Holocene history of the Greenland ice-sheet margin in northern Nunatarssuaq, northwest Greenland. Arktos 4, 10. https://doi.org/10.1007/s41063-018-0044-0.
Funder, S., Kjeldsen, K.K., Kjær, K.H., Cofaigh, C., 2011. The Greenland ice sheet during the last 300,000 years: a review. Dev. Quat. Sci. 15, 699–713.
Geirsdóttir, Á., Miller, G.H., Larsen, D.J., Ólafsdóttir, S., 2013. Abrupt Holocene climate transitions in the northern North Atlantic region recorded by synchronized lacustrine records in Iceland. Quat. Sci. Rev. 70, 48–62.
Gibbons, A.B., Megeath, J.D., Pierce, K.L., 1984. Probability of moraine survival in a succession of glacial advances. Geology 12, 327–330.
Grove, J.M., 1988. The Little Ice Age. Methuen, New York.
Heim, A., 1911. Uber die Petrographie und Geologie der Umgebungen von Karsuarsuk, Nordseite der halbinsel Nugsuak, W. Grönland. Meddelelser om Grønland, Bd. 47. Nr. 3.
Hippe, K., 2017. Constraining processes of landscape change with combined *in situ* cosmogenic ^{14}C-^{10}Be analysis. Quat. Sci. Rev. 172, 1–19.
Hippe, K., Lifton, N.A., 2014. Calculating isotope ratios and nuclide concentrations for *in situ* cosmogenic ^{14}C analyses. Radiocarbon 56, 1167–1174.
Ingólfsson, O., Frich, P., Funder, S., Humlum, O., 1990. Paleoclimatic implications of an early Holocene glacier advance on Disko-Island, West Greenland. Boreas 19, 297–311.
Ivy-Ochs, S., Kerschner, H., Maisch, M., Christi, M., Kubik, P.W., Schlüchter, C., 2009. Latest Pleistocene and Holocene glacier variations in the European Alps. Quat. Sci. Rev. 28, 2137–2149.
Jennings, A., Andrews, J., Pearce, C., Wilson, L., Ólfasdótttir, S., 2015. Detrital carbonate peaks on the Labrador shelf, a 13–7 ka template for freshwater forcing from the Hudson Strait outlet of the Laurentide Ice Sheet into the subpolar gyre. Quat. Sci. Rev. 107, 62–80.
Jomelli, V., et al., 2016. Paradoxical cold conditions during the medieval climate anomaly in the western Arctic. Sci. Rep. 6 https://doi.org/10.1038/srep32984.
Kaplan, M.R., Wolfe, A.P., Miller, G.H., 2002. Holocene environmental variability in southern Greenland inferred from lake sediments. Quat. Res. 58, 149–159.
Kaufman, D.S., et al., 2004. Holocene thermal maximum in the western Arctic (0–180°W). Quat. Sci. Rev. 23, 529–560.
Kelly, M.A., Lowell, T.V., 2009. Fluctuations of local glaciers in Greenland during latest Pleistocene and Holocene time. Quat. Sci. Rev. 28, 2088–2106.
Kelley, S.E., Briner, J.P., Young, N.E., 2013. Rapid ice retreat in Disko Bugt supported by ^{10}Be dating of the last recession of the western Greenland Ice Sheet. Quat. Sci. Rev. 82, 13–22.
Kelley, S.E., Briner, J.P., Zimmerman, S.R., 2015. The influence of ice marginal setting on early Holocene retreat rates in central West Greenland, early Holocene retreat rates in central West Greenland. J. Quat. Sci. 30, 271–280.
Kobashi, T., et al., 2017. Volcanic influence on centennial to millennial Holocene Greenland temperature change. Sci. Rep. 7 https://doi.org/10.1038/s41598-017-01451-7.
Larsen, D.J., Miller, G.H., Geirsdóttir, Á., 2013. Asynchronous little ice age glacier fluctuations in Iceland and European Alps linked to shifts in subpolar North Atlantic circulation. Earth Planet. Sci. Lett. 380, 52–59.
Larsen, N.K., Strunk, A., Levy, L.B., Olsen, J., Bjørk, A., Lauridsen, T.L., Jeppesen, E., Davidson, T.A., 2017. Strong altitudinal control on the response of local glaciers to Holocene climate change in southwest Greenland. Quat. Sci. Rev. 168, 69–78.
Larsen, L.M., Pedersen, A.K., Tegner, C., Duncan, R.A., Hald, N., Larsen, J.G., 2016. Age of Tertiary volcanic rocks on the West Greenland continental margin: volcanic evolution and event correlation to other parts of the North Atlantic Igneous Province. Geol. Mag. 3, 487–511.
Le Roy, M., Deline, P., Carcaillet, J., Schimmelpfennig, I., Ermini, M., ASTER Team, 2017. ^{10}Be exposure dating of the timing of Neoglacial glacier advances in the Ecrins-Pelvoux massif, southern French Alps. Quat. Sci. Rev. 178, 118–138.
Lesnek, A.J., Briner, J.P., 2018. Response of a land-terminating sector of the western Greenland Ice Sheet to early Holocene climate change. Evidence from ^{10}Be dating in the Søndre Isortoq region. Quat. Sci. Rev. 180, 145–156.
Levy, L.B., Kelly, M.A., Lowell, T., Hall, B., Hempel, L.A., Honsaker, W., Lusas, A.R., Howley, J.A., Axford, Y., 2014. Holocene fluctuations of Bregne ice cap, Scoresby Sund, east Greenland: a proxy for climate along the Greenland Ice Sheet margin. Quat. Sci. Rev. 92, 357–368.
Licciardi, J.M., 2000. Alpine Glacier and Pluvial Lake Records of Late Pleistocene Climate Variability in the Western United States. Ph.D. dissertation. Oregon State University, Corvallis, p. 155.
Lifton, N., Goehring, B., Wilson, J., Kubley, T., Caffee, M., 2015. Progress in automated extraction and purification of *in situ* ^{14}C from quartz: results from the Purdue *in situ* ^{14}C laboratory. Nuclear instruments and methods in physics research section B. Beam interactions with materials and atoms, 361, 381–386.
Lifton, N., Sato, T.,, Dunai, T.J., 2014. Scaling *in situ* cosmogenic nuclide production rates using analytical approximations to atmospheric cosmic-ray fluxes. Earth Planet. Sci. Lett. 386, 149–160. https://doi.org/10.1016/j.epsl.2013.10.052.
Lifton, N., 2016. Implications of two Holocene time-dependent geomagnetic models for cosmogenic nuclide production rate scaling. Earth Planet. Sci. Lett. 433, 257–268.
Lowell, T.V., Hall, B.L., Kelly, M.A., Bennike, O., Lusas, A.R., Honsaker, W., Smith, C.A., Levy, L.B., Travis, S., Denton, G.H., 2013. Late Holocene expansion of Istorvet ice cap, Liverpool Land, east Greenland. Quat. Sci. Rev. 63, 128–140.
Luckman, B.H., 2000. The little ice age in the Canadian rockies. Geomorphology 32, 357–384.
Marcott, S.A., Shakun, J.D., Clark, P.U., Mix, A.C., 2013. A reconstruction of regional and global temperature for the past 11,300 years. Science 339, 1198–1201.
Margreth, A., Dyke, A.S., Gosse, J.C., Telka, A.M., 2014. Neoglacial ice expansion and late Holocene cold-based ice cap dynamics on Cumberland Peninsula, Baffin Island, Arctic Canada. Quat. Sci. Rev. 91, 242–256.
Menounos, B., Osborn, G., Clague, J.J., Luckman, B.H., 2009. Latest Pleistocene and Holocene glacier fluctuations in western Canada. Quat. Sci. Rev. 28, 2049–2074.
Miller, G.H., Briner, J.P., Refsnider, K.A., Lehman, S.J., Geirsdóttir, Á., Larsen, D.J., Southon, J.R., 2013b. Substantial agreement on the timing and magnitude of Late Holocene ice cap expansion between East Greenland and the eastern Canadian Arctic: a commentary on Lowell et al. Quat. Sci. Rev. 77, 239–245, 2013b.
Miller, G.H., Geirsdóttir, Á., Zhong, Y., Larsen, D.J., Otto-Bliesner, B.L., Holland, M.M., Bailey, D.A., Refsnider, K.A., Lehman, S.J., Southon, J.R., Anderson, C., Björnsson, H., Thordarson, T., 2012. Abrupt onset of the Little Ice Age triggered by volcanism and sustained by sea-ice/ocean feedbacks. Geophys. Res. Lett. 39, L02708.

Miller, G.H., Landvik, J.Y., Lehman, S.J., Southon, J.R., 2017. Episodic Neoglacial snowline descent and glacier expansion on Svalbard reconstructed from the C-14 ages of ice-entombed plants. Quat. Sci. Rev. 155, 67–78.
Miller, G.H., Lehman, S.J., Refsnider, K.A., Southon, J.R., Zhong, Y.F., 2013a. Unprecedented recent summer warmth in Arctic Canada. Geophys. Res. Lett. 40, 5745–5751.
Möller, P., Larsen, N.K., Kjær, K.H., Funder, S., Schomacker, A., Linge, H., Fabel, D., 2010. Early to middle Holocene valley glaciations on northernmost Greenland. Quat. Sci. Rev. 29, 3379–3398.
Moreno-Chamarro, E., Zanchettin, D., Lohmann, K., Jungclaus, J.H., 2016. Internally generated decadal cold events in the northern North Atlantic and their possible implications for the demise of the Norse settlements in Greenland. Geophys. Res. Lett. 42, 908–915.
Moros, M., Andrews, J.T., Eberl, D.D., Jansen, E., 2006. Holocene history of drift ice in the northernNorth, northern North Atlantic: evidence for different spatial and temporal modes. Paleoceanography 21, PA2017.
Moros, M., et al., 2016. Surface and sub-surface multiproxy reconstruction of middle to late Holocene palaeoceanographic changes in Disko Bugt, West Greenland. Quat. Sci. Rev. 132, 146–160.
Nesje, A., 1992. A piston corer for lacustrine and marine sediments. Arct. Alp. Res. 257–259.
Nesje, A., 2009. Latest Pleistocene and Holocene alpine glacier fluctuations in Scandinavia. Quat. Sci. Rev. 28, 2119–2136.
Nishiizumi, K., Imamura, M., Caffee, M.W., Southon, J.R., Finkel, R.C., McAninch, J., 2007. Absolute calibration of ^{10}Be AMS standards: Nuclear instruments and methods in physics research section. Phys. Res. Sect. B: Beam Interact. Mater. Atoms 258, 403–413.
Noh, M.J., Howat, I.M., 2015. Automated stereo-photogrammetric DEM generation at high latitudes, latitudes: surface Extraction from TIN-Based Search Minimization (SETSM) validation and demonstration over glaciated regions. GISci. Rem. Sens. 52, 198–217.
O'Hara, S.L., Briner, J.P., Kelley, S.E., 2017. A ^{10}Be chronology of early Holocene local glacier moraines in central West Greenland. Boreas 46, 655–666.
Oerlemans, J., 2005. Extracting a climate signal from 169 glacier records. Science 308, 675–677.
Paillard, D., Labeyrie, L.D., Yiou, P., 1996. AnalySeries 1.0: a Macintosh software for the analysis of geophysical time-series. EOS T Am Geophys Un 77, 379.
Pendleton, S.L., Miller, G.H., Anderson, R.A., Crump, S.E., Zhong, S.E., Yafang, Z., Jahn, A., Geirsdóttir, Á., 2017. Episodic Neoglacial expansion and rapid 20th century retreat of a small ice cap on Baffin Island, Arctic Canada, and modeled temperature change. Clim. Past 13, 1527–1537.
Perner, K., Moros, M., Jennings, A., Lloyd, J.M., Knudsen, K.L., 2013. Holocene paleoceanographic evolution off West Greenland, paleoceanographic evolution off West Greenland. The Holocene 23, 374–387.
Phillips, F.M., Argento, D.C., Balco, G., Caffee, M.W., Clem, J., Dunai, T.J., Finkel, R., Goehring, B., Gosse, J.C., Hudson, A.M., Jull, A.T., 2016. The CRONUS-Earth project: a synthesis. Quat. Geochronol. 31, 119–154.
R Development Core Team, 2012. R: A Language and Environment for Statistical Computing. R Foundation for Statistical Computing, Vienna, Austria.
Rasmussen, S.O., Vinther, B.M., Clausen, H.B., Andersen, K.K., 2007. Early Holocene climate oscillations recorded in three Greenland Ice cores. Quat. Sci. Rev. 26, 1907–1914.
Reimer, P.J., Bard, E., Bayliss, J.W., Beck, P.G., Blackwell, C., Bronk Ramsey, C.E., Buck, H., Cheng, R.L., Edwards, M., Friedrich, P.M., Grootes, T.P., Guilderson, H., Haflidason, I., Hajdas, C., Hatte, T.J., Heaton, D.L., Hoffmann, A.G., Hogg, K.A., Hughen, K.F., Kaiser, B., Kromer, S.W., Manning, M., Niu, R.W., Reimer, D.A., Richards, E.M., Scott, J.R., Southon, R.A., Staff, C., Turney, S.M., van der Plicht, J., 2013. IntCal13 and Marine13 radiocarbon age calibration curves -50,000 years cal BP. Radiocarbon 55, 1869–1887.
Rein, B., Sirocko, F., 2002. In-situ reflectance spectroscopy–analyzing techniques for high resolution pigment logging in sediment cores. Int. J. Earth Sci. 91, 950–954.
Roberts, D.H., Rea, B.R., Lane, T.P., Schnabel, C., Rodés, A., 2013. New constraints on Greenland ice sheet dynamics during the last glacial cycle: evidence from the Uummannaq ice stream system. J. Geophys. Res. 118, 519–541.
Røthe, T.O., Bakke, J., Vasskog, K., Gjerde, M., D'Andrea, W.J., Bradley, R.S., 2015. Arctic Holocene glacier fluctuations reconstructed from lake sediments at Mitrahalvøya, Spitsbergen. Quat. Sci. Rev. 109, 111–125.
Schimmelpfennig, I., Schaefer, J.M., Akcar, N., Ivy-Ochs, S., Finkel, R.C., Schlüchter, C., 2012. Holocene glacier culminations in the Western Alps and their hemispheric relevance. Geology 40, 891–894.
Schweinsberg, A.D., Briner, J.P., Miller, G.H., Bennike, O., Thomas, E.K., 2017. Local glaciation in west Greenland linked to North Atlantic Ocean circulation during the Holocene. Geology 45, 195–198.
Schweinsberg, A.D., Briner, J.P., Miller, G.H., Lifton, N.A., Bennike, O., Graham, B.L., 2018. Holocene mountain glacier history in the Sukketoppen Iskappe area, Southwest Greenland. Quat. Sci. Rev. 197, 142–161.
Sigl, M., et al., 2015. Timing and climate forcing of volcanic eruptions for the past 2,500 years. Nature 523, 543–549.
Solomina, O.N., et al., 2015. Holocene glacier fluctuations. Quat. Sci. Rev. 111, 9–34.
Solomina, O.N., et al., 2016. Glacier fluctuations during the past 2000 years. Quat. Sci. Rev. 149, 61–90.
Stuiver, M., Reimer, P.J., Reimer, R., 2005. CALIB Radiocarbon Calibration. Execute version, 5(2).
Sugden, D.E., 1972. Deglaciation and isostasy in the Sukkertoppen ice cap area, west Arct, Greenland. Alp. Res. 4, 97–117.
Swingedouw, D., Ortega, P., Mignot, J., Guilyardi, E., Masson-Delmotte, V., Butler, P.G., Khodri, M., Seferian, R., 2015. Bidecadal North Atlantic ocean circulation variability controlled by timing of volcanic eruptions. Nat. Commun. 6, 6545.
Thomas, E.K., Szymanski, J., Briner, J.P., 2010. Holocene alpine glaciation inferred from lacustrine sediments on northeastern Baffin Island, Arctic Canada. J. Quat. Sci. 25, 146–161.
Van der Bilt, W.G.M., Rea, B., Spagnolo, M., Roerdink, D.L., Jorgensen, S.L., Bakke, J., 2018. Novel sedimentological fingerprints link shifting depositional processes to Holocene climate transitions in East Greenland. Glob. Planet. Chang. 164, 52–64.
Vasskog, K., Paasche, Ø., Nesje, A., Boyle, J.F., Birks, H.J.B., 2012. A new approach for reconstructing glacier variability based on lake sediments recording input from more than one glacier. Quat. Sci. Rev. 77, 192–204.
Vaughan, D.G., Comiso, J.C., Allison, I., Carrasco, J., Kaser, G., Kwok, R., Mote, P., Murray, T., Paul, F., Ren, J., Rignot, E., Solomina, O., Steffen, K., Zhang, T., 2013. Observations: cryosphere. In: Climate Change 2013: the Physical Science Basis. Contribution of Working Group I to the Fifth Assessment Report of the Intergovernmental Panel on Climate Change. IPCC.
Weidick, A., 1968. Observations on some Holocene glacier fluctuations in West Greenland. Meddelelser om Grønland 165, 1–202.
Weidick, A., Bennike, O., 2007. Quaternary glaciation history and glaciology of Jakobshavn Isbræ and the Disko Bugt region, West Greenland: a review. Geol. Surv. Den. Greenl. Bull. 14, 1–78.
Winsor, K., Carlson, A.E., Rood, D.H., 2014. ^{10}Be dating of the Narsarsuaq moraine in southeast, southeast Greenland: evidence for a late-Holocene ice advance exceeding the Little Ice Age maximum. Quat. Sci. Rev. 98, 135–143.
Wolfe, A.P., Cooke, C.A., Hobbs, W.O., 2006. Are current rates of atmospheric nitrogen deposition influencing lakes in the eastern Canadian Arctic? Arctic Antarct. Alpine Res. 38, 465–476.
Young, N.E., Briner, J.P., Rood, D.H., Finkel, R.C., Corbett, L.B., Bierman, P.R., 2013a. Age of the Fjord Stade moraines in the Disko Bugt region, western Greenland, and the 9.3 and 8.2 ka cooling events. Quat. Sci. Rev. 60, 76–90.
Young, N.E., Schaefer, J.M., Briner, J.P., Goehring, B.M., 2013b. A ^{10}Be production rate calibration for the Arctic. J. Quat. Sci. 28, 515–526.
Young, N.E., Schweinsberg, A.D., Briner, J.P., Schaefer, J.M., 2015. Glacier maxima in Baffin Bay during the medieval warm period coeval with Norse settlement. Sci. Adv. 1, e1500806.